Automation in Construction xxx (xxxx) xxx

Contents lists available at ScienceDirect

Automation in Construction

journal homepage: www.elsevier.com/locate/autcon

Q4

Highlights

Automation in Construction xxx (2019) xxx–xxx

Dimensional accuracy, flowability, wettability, and porosity in inkjet 3DP for gypsum and cement mortar materials

Pshtiwan Shakor[a,*], Shami Nejadi[a], Gavin Paul[b], Jay Sanjayan[c]

[a] Centre for Built Infrastructure Research, School of Civil and Environmental Engineering, Faculty of Engineering and IT, University of Technology Sydney, Ultimo, NSW 2007, Australia
[b] Centre for Autonomous Systems, School of Mechanical and Mechatronic Engineering, Faculty of Engineering and IT, University of Technology Sydney, Ultimo, NSW 2007, Australia
[c] Centre for Sustainable Infrastructure, Faculty of Science, Engineering and Technology, Swinburne University of Technology, Hawthorn, VIC 3122, Australia

- kjet 3D printing using cement mortar is presented, along with the measurement and comparison of the printed specimens' dimensional accuracy in all three planes.
- Studied the flowability of the dry cementitious powder and the commercial powder (gypsum).
- Investigated the wettability of the powder-bed by conducting liquid droplet penetration tests.
- Measured the porosity of the powder-bed and the apparent porosity of the printed specimens.
- Performed a detailed characterization of cementitious and gypsum powders used in inkjet 3D printing.

https://doi.org/10.1016/j.autcon.2019.102964
0926-5805/Crown Copyright © 2019 Published by Elsevier B.V. All rights reserved.

Please cite this article as: P. Shakor, S. Nejadi, G. Paul, et al., Dimensional accuracy, flowability, wettability, and porosity in inkjet 3DP for gypsum and cement mor..., Automation in Construction, https://doi.org/10.1016/j.autcon.2019.102964

UNCORRECTED PROOF

Video 1 Flowing CP powder particles from the feeder container onto the feeder chamber.

Video 2 Flowing ZP 151 powder particles from the feeder container onto the feeder chamber.

Automation in Construction xxx (xxxx) xxx

Contents lists available at ScienceDirect

Automation in Construction

journal homepage: www.elsevier.com/locate/autcon

Dimensional accuracy, flowability, wettability, and porosity in inkjet 3DP for gypsum and cement mortar materials

Pshtiwan Shakor [a,*], Shami Nejadi [a], Gavin Paul [b], Jay Sanjayan [c]

[a] Centre for Built Infrastructure Research, School of Civil and Environmental Engineering, Faculty of Engineering and IT, University of Technology Sydney, Ultimo, NSW 2007, Australia
[a] Centre for Autonomous Systems, School of Mechanical and Mechatronic Engineering, Faculty of Engineering and IT, University of Technology Sydney, Ultimo, NSW 2007, Australia
[c] Centre for Sustainable Infrastructure, Faculty of Science, Engineering and Technology, Swinburne University of Technology, Hawthorn, VIC 3122, Australia

ARTICLE INFO

Article history:
Received 22 May 2019
Received in revised form 26 August 2019
Accepted 10 September 2019
Available online xxxx

Keywords:
Dimensional accuracy
Flowability
Wettability
Porosity
Cement mortar
Inkjet 3DP

ABSTRACT

Inkjet (powder-based) 3D Printing is a popular and widely used technology, which can be applied to print a wide range of specimens using different powder materials. This paper discusses the use of inkjet 3DP technology for construction applications using custom-made powder instead of commercial gypsum powder (ZP 151). The paper aims to address the differences between ZP 151 and CP (a custom-made construction-specific cement mortar powder) with regard to powder flowability, wettability, powder bed porosity and apparent porosity in 3DP specimens. An inkjet 3D printer is employed and experimental results verify that ZP 151 has a lower angle of repose, a higher contact angle and noticeably less porosity in the powder bed compared with the CP powder. Additionally, specimens printed with ZP 151 have a lower apparent porosity compared with CP specimens. The wettability for each of the powders was tested using contact angle goniometer, while the Optronis CamRecorder was used at 1000 fps at 800 × 600 pixel resolution images for the powder flowability tests. The bulk density tester was utilised to find the apparent porosity in the printed specimens. The paper also discusses the details of the printing procedure and dimensional accuracy of printed specimens.

Crown Copyright © 2019 Published by Elsevier B.V. All rights reserved.

1. Introduction

Concrete members and structures that contain steel or reinforcement are satisfactory for use as structurally reinforced components in the construction industry [1]. The construction industry continues to apply conventional methods to build structural members such as beams and columns [2]. These structural members can be reinforced using steel [3] or by improving the stiffness of concrete using fibre reinforcement [4–7]. However, the conventional methods need to be updated to take advantage of technological advancements that enable increased dimensional accuracy in the concrete structures, increase workplace safety, and allow the construction of uniquely-shaped objects, which are cost-effective and permit the application of complex geometries to concrete applications [8–14].

Currently, Additive Manufacturing (AM) is an advanced technology that can be applied to solve challenges in the construction industry. Recent applications of AM include inkjet (powder-based) three-dimensional printing (3DP) and extrusion concrete printing (by means of a robot or 3-axis moveable frame) [15–17]. Many studies focus on the printing process via a robotic arm and 3-axis gantry frame [18–23] but they generally lack a detailed explanation of the inkjet printing process.

Inkjet 3DP is more suitable compared to other additive manufacturing techniques for precast members. It can be easily applied to precast concrete members or whole structural buildings with further post-processing. The inkjet printing technique has advantages over other techniques, for example, extrusion-based techniques. One advantage of the inkjet technique over extrusion is that the printing process does not require much monitoring for the mixing materials. In the extrusion-based technique, the procedure should be carefully handled and monitored during both the mixing and the printing process. The wet state mixing in extrusion printing often causes the materials to prematurely set within the delivery systems, leading to challenges with depositing the slurry materials. On the other hand, the inkjet printing process consists of infusing water with layered dry powder without additional manual intervention. Therefore, having enough materials in the feeder tank is all that is required for the printer to be left to complete the entire structure. In recent work, it has been shown that the mechanical strength of the inkjet 3DP specimen can be increased by adding additional post-processing steps such as heat curing for the specimen before or after wet curing [24–26].

The inkjet 3DP process also overcomes many obstacles while printing, for example, the reinforcement, flowability and wettability of the particles, which are the most vital factors in this technique as they affect

* Corresponding author.
E-mail addresses: pshtiwan.shakor@uts.edu.au (P. Shakor), shami.nejadi@uts.edu.au (S. Nejadi), gavin.paul-1@uts.edu.au (G. Paul), jsanjayan@swin.edu.au (J. Sanjayan).

https://doi.org/10.1016/j.autcon.2019.102964
0926-5805/Crown Copyright © 2019 Published by Elsevier B.V. All rights reserved.

Please cite this article as: P. Shakor, S. Nejadi, G. Paul, et al., Dimensional accuracy, flowability, wettability, and porosity in inkjet 3DP for gypsum and cement mor..., Automation in Construction, https://doi.org/10.1016/j.autcon.2019.102964

UNCORRECTED PROOF

ARTICLE IN PRESS

the accuracy, resolution and spreadability of the powder [11,27–31]. Particularly, this technique is a new technology in mortar and concrete applications. The physical and chemical interaction of cementitious materials faces many challenges and numerous difficulties.

The flowability of a powder is an essential parameter that must be known and kept uniform during the additive manufacturing process of inkjet 3DP. Highly flowable powder increases the resolution of the final printed product, while powders with low flowability can reduce the resolution of the printed part [32]. In the earlier works, there have not been any comparative studies for the cement mortar materials and plaster powder (ZP151) in inkjet 3DP technology. In this paper, the differences between the two powders, namely, plaster powder (ZP 151) from 3DSystems or Zcorp manufacturer and the modified powder cement mortar (CP) are discussed. These powders were tested for flowability purposes, and to determine the resolution of both the powder bed and the printed specimens.

The printhead of a 3DP has a major contribution to the resolution of the printed objects. Printheads are generally divided into two main groups: continuous inkjet (CIJ) printing and drop-on-demand (DOD) inkjet printing [33]. CIJ, which is used mostly for coding and marking purposes, uses liquid diameters usually between 10 and 150 μm, while DOD is used for graphics and text printing with liquid diameters typically between 20 and 50 μm [34]. In this study, the DOD type of cartridge has been used for the printing application.

The printhead of the inkjet 3DP (ProJet 360, ZP 150) is operated with an HP 11 printhead. The HP 11 printhead uses thermal DOD technology, with the ink leaving the reservoir only when required. The ink droplet directly affects the enveloped powder bed in the build chamber of the 3DP [35]. The drop penetration behaviour on the packed powder has a key effect on the quality of the printed parts. The drops from the nozzles of the printhead are ejected and selectively dropped on the packed powder to build a printed specimen [32]. The printability of the 3D part is also distinct from the characterization of the powder, which is an essential part of the 3DP process [32]. The characteristics of the powder particles are influenced by two main factors: firstly, the powder topology such as particle size, morphology, specific surface area and particle distribution; and secondly, the reaction of the material to the binder. Dropping the droplet into the powder can be divided into three stages: droplet penetration into powder pores; setting to form nucleation, and wetting next to powders [36]. The same study demonstrated that powder-binder wettability, the drop-spreading behaviours into the powder, and the reaction of the powder particles was a major factor in achieving a successful specimen prior to the 3DP techniques. These properties and the respective powder performances need to be determined for the cementitious materials in 3DP.

The main quality of surface resolution for the printed specimen depends on the characteristics of the powder and binder droplet. Zhou et al. [35] studied the surface roughness and the surface homogeneity of coarse and fine powders. They found that coarse powder has a higher level of surface homogeneity, while fine powder has a greater level of roughness. Panda et al. [37] proposed that a high volume of fly ash with added nano-attapulgite clay could improve the printability of materials in the extrusion-based printing. However, these powders might be unsuitable for inkjet 3D printers because the cementitious powders cause agglomerations if they remain in the feeder tank of the printer for extended periods. Hence, the roughness and porosity of the powder bed particles and printed parts have been presented in this paper for both the commercial materials and the custom-made materials.

The dimensional accuracy of the 3DP technique is another essential property, which must be investigated in more detail. Farzadi et al. [27] studied the dimensional accuracy of different layer thicknesses, namely, 0.0875 mm, 0.1 mm, 0.1125 mm and 0.125 mm. The results showed that the layer thickness of 0.1125 had the closest height dimension to the height dimensions of the CAD model. Another study by Kalms et al. [38] used a laser printed technique to determine the accuracy of the printed part, they found that the accuracy in the laser technique is better than 10 μm. Therefore, this paper reveals the dimensional accuracy of the cement mortar printed specimen in inkjet 3DP, which is not covered by earlier studies.

In the present study, the dimensional accuracy of each of the printed specimens is measured and examined in all dimensional axes. In addition, the effect of wettability on the printed specimens and the flowability of the powder particles through a feed container of the 3DP for each of the powders are investigated. Visual inspections of the surface resolutions are then performed. Finally, laser scanning and surface roughness tests are conducted.

2. Materials and methods

2.1. Materials characterization

2.1.1. Powder description

The commercial powder (ZP 151) from the 3DSystems manufacturer, has a high content of gypsum plaster (calcium sulphate hemihydrate). Cementitious (modified) powder (CP) consists of Ordinary Portland Cement (OPC), Calcium Aluminate Cement (CAC), Lithium Carbonate (Li_2CO_3) and Fine Sand as explained in the previous work [16]. Lithium Carbonate has been used as an agent to quicken the setting time of the cement [39].

ZP 151 powder, CAC and OPC have particle size distributions known as diameter D10, D50, and D90 where D10, D50 and D90 symbolize the midpoint and range of the particle size distribution (PSD). These categorisations are based on PSD analysis results with calculations for 10%, 50% and 90% of the mass, respectively. The tests were performed using a particle size analyser (Malvern 2000) and particle size laser distributor (Cilas 1190), see Table 1.

The mixed proportion of CP comprises 67.8% CAC and 32.2% OPC. The selection of materials has been explained in the authors' earlier studies [16,26]. After finding the particle size of each powder and then by heuristically determining the optimum mix, which is closest to the targeted commercial powder. Additionally, 4.5% of the total mix is comprised of lithium carbonate (accelerate agent Li_2CO_3). The lithium carbonate assists to produce rapid setting at a low cost, high early strength and provides excellent adhesion and stability [39]. Some of the specimens were prepared without lithium carbonate and instead of being replaced by 5% of fine sand.

The CAC powders were sieved using 150 to 75 μm sieves. The sieves were shaken for approximately 5 min. Next, the three powders (CAC, OPC, Lithium carbonate) were mixed properly using a Hobart mixer at a rotation speed of 1450 RPM (Revolution Per Minute) for approximately 10 min. The CAC and OPC powders have dissimilar PSD (i.e. OPC is finer than CAC), but it was blended appropriately to achieve one powder with a similar consistency to the recommended powder, which is used in the 3DSystems printers.

The inkjet-printed specimens were categorised into two different forms as shown in Fig. 1. Firstly, Fig. 1a shows that the shell and core were fully saturated, which is termed “different saturation” in inkjet 3DP. For example, S170C340 means shell 170%, core 340% with equal saturation levels/volumes for shell and core.

Fig. 1b shows the second form, which is a shell full saturated and core half saturated. This is termed “similar saturation” in inkjet 3DP. As before, the condensed form is used, e.g. S170C170 means shell

Table 1
Particle size distributions (PSD) for OPC, CAC, ZP 151 and fine sand.

Powder type	D10	D50	D90
Ordinary Portland cement	0.19 μm	8.93 μm	38.46 μm
Calcium aluminate cement	3.38 μm	79.93 μm	127.11 μm
ZP 151 (gypsum powder)	1.48 μm	23.07 μm	70.12 μm
Fine sand	83.23 μm	110.51 μm	147.89 μm
Lithium carbonate	1.63 μm	5.58 μm	13.56 μm

UNCORRECTED PROOF

Please cite this article as: P. Shakor, S. Nejadi, G. Paul, et al., Dimensional accuracy, flowability, wettability, and porosity in inkjet 3DP for gypsum and cement mor..., Automation in Construction, https://doi.org/10.1016/j.autcon.2019.102964

ARTICLE IN PRESS

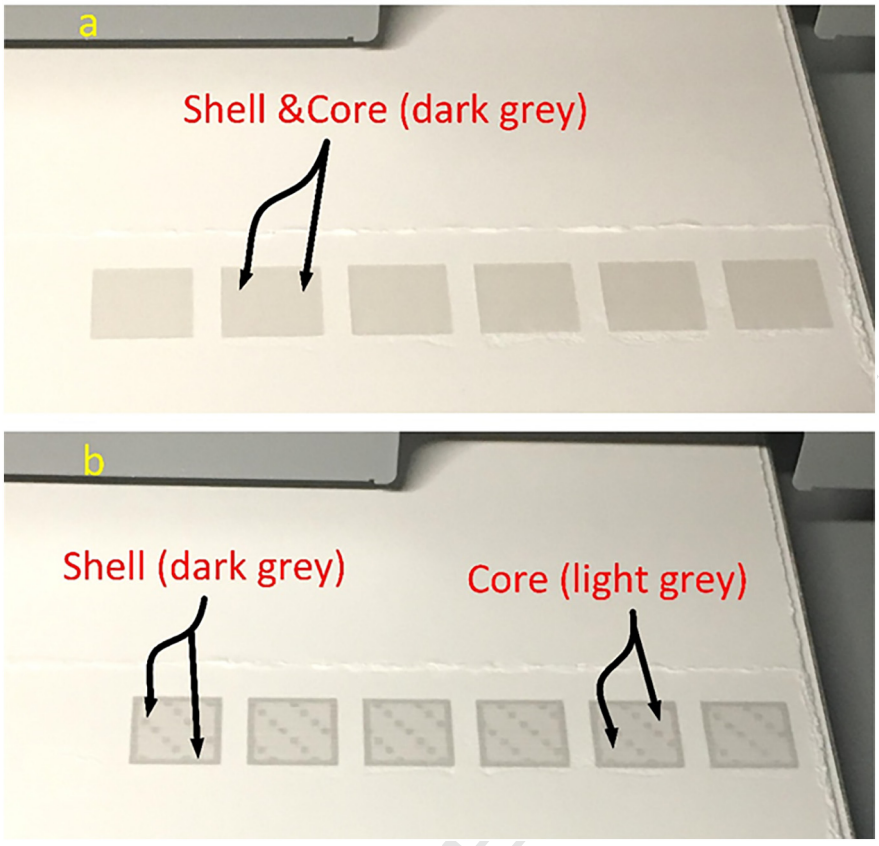

Fig. 1. Printing cube for ZP 151, (a) using a saturation level for shell and core (S170C340), (b) using a saturation level for shell and core (S170C170).

170%, core 170%, with full saturation for the shell and half-saturation for the core (see Table 2).

Table 2 shows the saturation level as a percentage (%) and the water/cement ratio (*w/c*) for each of the powders. This has been found according to Miyanaji et al. [40] and defined by Eq. (1), where V_b is the volume of binder and V_p is the volume of powder;

$$Saturation\ level = V_b/V_p \quad (1)$$

2.1.2. Reactive agent

The reactive agent used in this test is commercially known as a Z Clear Binder Cartridge (zb®63). The major content of this liquid is water and humectant [41]. The 3D printing procedure was executed on a 3D printer (ProJet CJP 360, 3DSystems) with a print head HP11 (C4810A). The printer has a resolution of 300 × 450 dpi, see Table 3. This study used a similar liquid which is called *Z*-binder (Zb 63). Two studies, with a ZPrinter [42] and [43], used a similar liquid with a surface tension of 0.00045 N/cm and a viscosity of 0.0135 g/cm-s. Water has a surface tension of 0.00072 N/cm and this can be decreased by adding agent (e.g. Isopropyl Alcohol) to ease the flow of water as it passes through the printer head (cartridge).

2.2. Specimen preparation

The ZP 151 and CP powders were separately loaded into the 3DP machine's feeder buckets in preparation for the printing process. The printhead of the ProJet CJP 360 drops a binder liquid into the powder using the conventional inkjet technique. Table 4 presents the essential specifications of the printed specimens modelled in SolidWorks software.

Printing was executed with binder/volume ratios of 0.415 for the shell (S) and core (C) with a saturation level of (S175C340) %. This ratio was chosen based on the research findings in Shakor et al. [16], where it was found to produce the optimum result for the mechanical behaviours of the structural elements. The ratio of binder/volume for the shell and core regions was proposed as a constant and a similar test setup was used for all the specimens.

After printing was completed, the fabricated models were dried in the build chamber for 90 min before being taken out of the powder bed. Next, the specimens were depowdered using a vacuum to remove any unbound powder. Fig. 2 shows the resulting real 3DP specimens, where it can be seen that the printed parts for CP have a filleted edge compared to the edges in the ZP 151 specimen.

Table 2
Saturation levels, volume of binder to volume of powder and *w/c* for ZP 151 and CP.

Saturation level %	V_b/V_p	*w/c*	
		ZP 151	CP
S100C200	0.244	0.27	0.31
S125C250	0.305	0.33	0.38
S150C300	0.366	0.40	0.46
S170C350	0.415	0.46	0.52

Table 3
Physical and chemical properties of zb®63 binder.

Description	Density (g/cm^3)	Surface tension (N/cm)	Viscosity (g/cm-s)	pH (20 °C)
zb®63 binder	1	0.00045	0.0135	9.8

Please cite this article as: P. Shakor, S. Nejadi, G. Paul, et al., Dimensional accuracy, flowability, wettability, and porosity in inkjet 3DP for gypsum and cement mor..., Automation in Construction, https://doi.org/10.1016/j.autcon.2019.102964

ARTICLE IN PRESS

t4.1 **Table 4**
t4.2 Printed specimens and the number of specimens for each of the specified tests.

t4.3 t4.4 Specimen description	Number of specimens for compressive strength (28 days)	Number of specimens for porosity measurement with Li_2CO_3	Number of specimens for porosity measurement without Li_2CO_3	Number of specimens for dimensional test
t4.5 S100C200	3	3	3	10
t4.6 S125C250	3	3	3	10
t4.7 S150C300	3	3	3	10
t4.8 S170C340	3	3	3	10

2.3. Printer feeder bin and feeder chamber

The inkjet 3DP consists of three main parts: the feeder chamber, build chamber and feeding container Fig. 3.

Table 5 shows the build chamber volume and cleaning unit for the inkjet 3DP.

In the feeder container, there is a rotor which rotates in clockwise and anticlockwise directions at a speed of 30 RPM. The length of the rotor shaft, which consists of 4 parallel stainless-steel bars, is 290 mm, as shown in Fig. 4. Inside the feeder container, there are 21 rectangular holes with dimensions of 4.5 × 1 mm. The particles of the powder flow down to the feed chamber through these holes.

2.4. Dimensional accuracy

The dimensions of the 3DP cubes were measured using digital callipers, which measures all three-sides of the specimens with an accuracy of 0.01 mm. Also, a MeasumaX, which has an accuracy of ±0.04 mm, was used to measure the height of the specimens. The real measurements can then be compared with the CAD model drawn using SolidWorks software.

2.5. Flowability of the powder

To fill the powder in the build chamber, enough powder is required to be packed in the bed so that it is homogeneously spread through the build chamber. Powder flowability is the most important factor in this procedure to make a suitable spread over the feeder and build chamber. Major factors that influence the flowability include particle size, the surface area of the powder, surface roughness and the printed layer thickness.

Powder flowability can be described as the capability of a powder to flow. Flowability can be expressed as a one-dimensional representation of powder, by which powders can be graded on a scale from free-flowing to nonflowing [44].

The funnel, beaker, measuring cylinder and funnel holding stand were used in this study. According to Gold et al. [45], the flow test and angle of repose has accurate requirements for the precision of the equipment and its calibration. The gypsum and cementitious powder flow through the orifice outlet (Ø 5 ± 0.13 mm) of the flowmeter funnel, which controls the rate of powder flow. The flowmeter test was conducted to check the consistency of the powder flow and to investigate its success in building powder particles. In the case where some powder does not flow effortlessly, and then further blending is required before it is used in the machine. However, if the powder reaches the required flow, it can be used for the machine [46].

2.6. Wettability

To discover the wettability of the powder, it is crucial to first determine two particular powder properties. Table 6 shows the powder properties of bulk density and surface area for ZP 151 and CP. The surface area for CP is higher than the surface area for ZP 151, which suggests that a greater reaction could possibly occur for CP than for ZP 151. Additionally, Table 6 shows that there are a higher number of particles on the surface of the powder in CP than ZP 151. This is directly related to the wettability of the powder. However, the layer thickness on the build chamber has a major impact on the binder penetration and the spreadability of the binder over the packed powder. As shown in

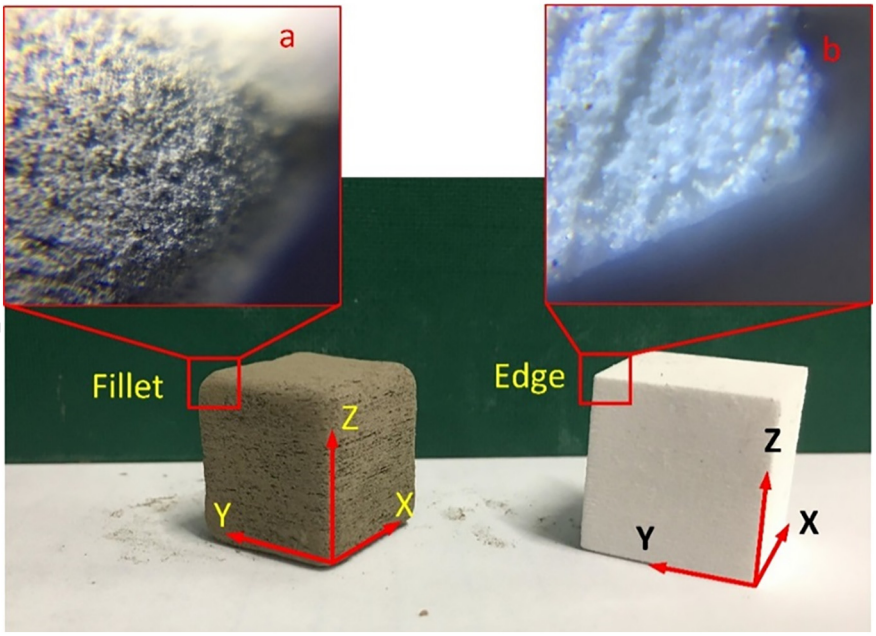

Fig. 2. Cement mortar cube (CP) (20 × 20 × 20 mm) (a), Gypsum cube (ZP 151) (20 × 20 × 20 mm) (b) printed by ProJet 360.

Please cite this article as: P. Shakor, S. Nejadi, G. Paul, et al., Dimensional accuracy, flowability, wettability, and porosity in inkjet 3DP for gypsum and cement mor..., Automation in Construction, https://doi.org/10.1016/j.autcon.2019.102964

ARTICLE IN PRESS

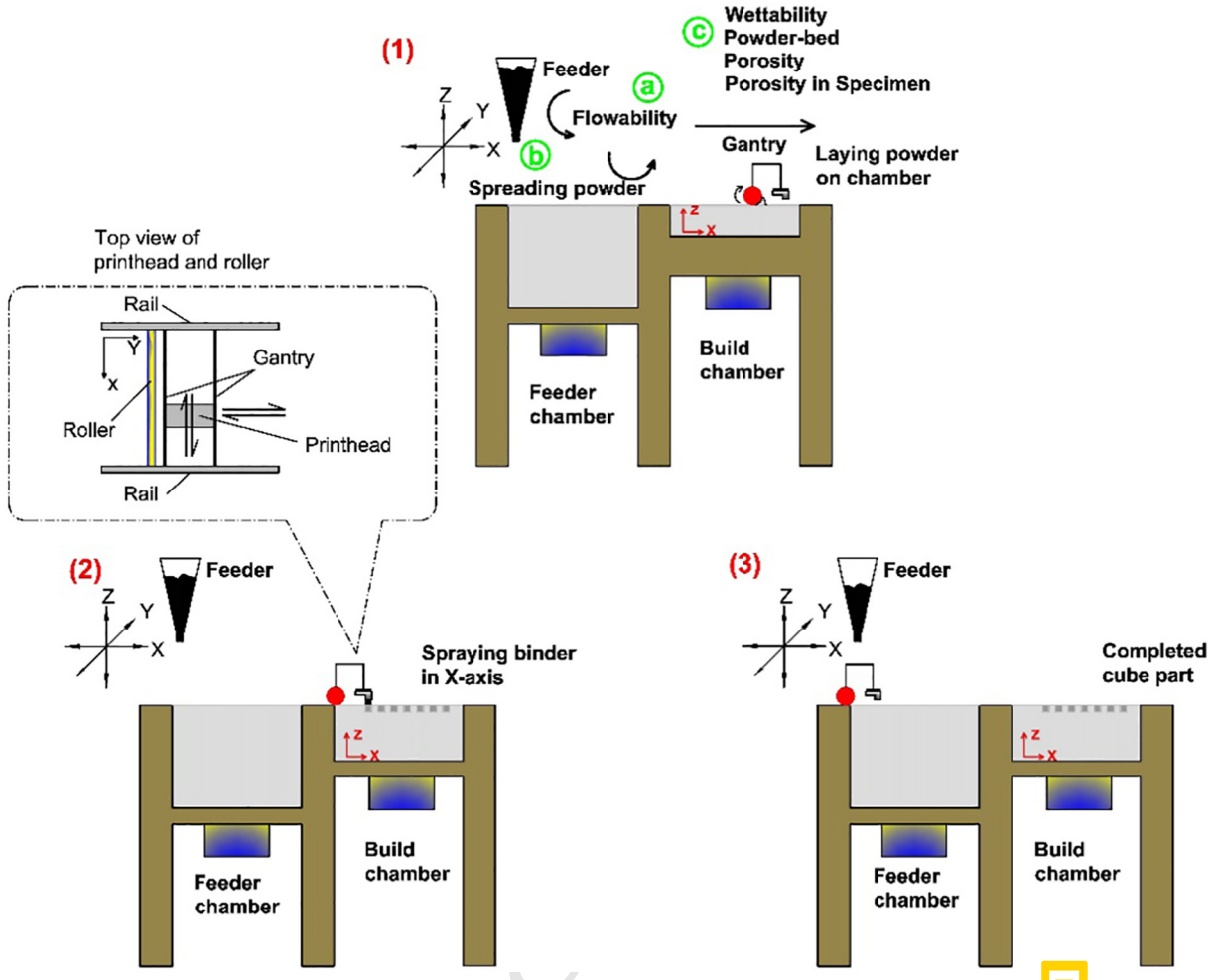

Fig. 3. Schematic illustration of the inkjet 3D printing process from (1 to 3): (a) Flowability from the feeder tank; (b) Spreading powder on feeder chamber; (c) Spreading powder on build chamber, This depends on the wettability, and the porosity of both the powder bed and the printed parts.

Table 6, the bulk density of ZP 151 is greater than the bulk density of CP. This means that the porosity of ZP 151 is lower than it is for CP as presented in the study [47], where it was found that increasing the bulk density of the powder significantly decreased the porosity of the powder.

2.7. Powder bed porosity

The tests were prepared using Accupyc II (gas pycnometer) to measure the true density. The true density (ρ_{true}) and bulk density (ρ_{bulk}) of the powders were measured according to Australian Standards [48]. Eq. (2) is used to calculate the powder bed porosity in the build chamber of the printer;

$$P_{bed} = 1 - \frac{\rho_{bed}}{\rho_{true}} \times 100\% \quad (2)$$

In-process bed density (ρ_{bed}), was proposed by Zhou et al. [35]. This measures the density after the powder is spread on the build chamber. To ensure high-quality printing, it is vital to have the high-quality spreading of powder particles in the build chamber of the 3D printer.

Table 5
ProJet 360 build size dimensions.

Model	Colour	Cleaning	Build volume
ProJet® 360	Monochrome	Built-in	203 × 254 × 203 mm

2.8. Porosity in the specimen

The apparent porosity test for the solid specimen in the 3DP parts is an important test to measure the voids and porosity of the specimen. Apparent porosity tests have been performed according to the Australian Standard on the specimens as presented in Table 4 [49]. All experiments were performed in the laboratory on cubic specimens using the XQK tester machine. The specimens were dried in an oven at 105 °C for approximately 2 h. The specimen weight at this stage is labelled as dry weight (m_1). Later, specimens were put in a porosity tester and the air inside the tester machine was evacuated. The machine tester was then filled with water until the specimens were covered by approximately 5 cm of water. The specimens were then left submerged for 10 min. Finally, the specimens were weighed. The weight of the specimens that had been submerged in the water was designated (m_2), then after the four sides of the specimens were rolled on a piece of wet fabric, the weight is denoted (m_3). Further details of this process are described in [16].

The apparent porosity (P_a) of cubes can be calculated using Eq. (3);

$$P_a = \frac{m_3 - m_1}{m_3 - m_2} \times 100 \quad (3)$$

UNCORRECTED

Please cite this article as: P. Shakor, S. Nejadi, G. Paul, et al., Dimensional accuracy, flowability, wettability, and porosity in inkjet 3DP for gypsum and cement mor..., Automation in Construction, https://doi.org/10.1016/j.autcon.2019.102964

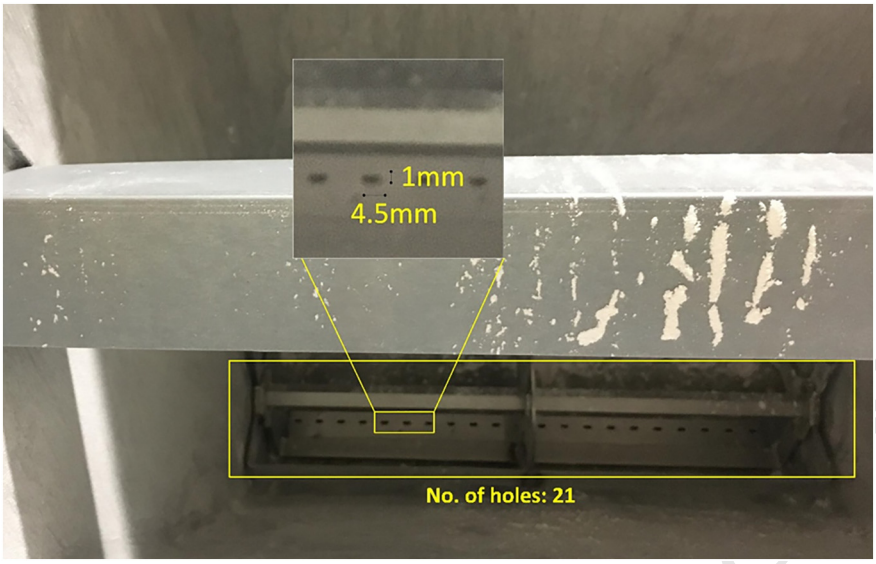

Fig. 4. Inside the feeder container showing the number of holes in the container.

3. Results and discussions

3.1. Materials characterization

3.1.1. Powder description

The powder particle size distribution (PSD) was measured for both the CP and the ZP 151 powder types. Three replicas were prepared for each material. The PSD test results are shown in Fig. 5. The graph shows the closeness of the cumulative distribution for the cement mortar powder (CP) compared to the commercial powder (ZP 151).

In the printing process, the printer parameters were set on a layer thickness of 0.1 mm and a default delay value time between layers of 100 ms.

3.1.2. Reactive agent

The binder is mainly water, which can react with gypsum powder and cementitious powder effortlessly, i.e. without any extra liquid solutions. The 3DP specimens with high porosity allowed the powder to absorb the binder, potentially leading the printed object to change dimensions and shrink. Thus, the produced 3DP specimen continuously can be expected to change its properties and dimensions over time in a variable environment such as medium temperature and humidity [50]. Since binder hardening usually occurs during the layer creation, the binder liquid transforms into a solid form which can result in shape inaccuracy and object shrinkage [51]. The binder contains humectant and some types of alcohol that helps the materials to become more hygroscopic and absorb moisture from the air. It is the nature of each type of cement to absorb moisture from the air. Therefore, the ambience significantly affects the resulting printed part.

3.2. Printer feeder container and feeder chamber

The feeder container includes the rotor, which revolves to push the materials down into the feeder chamber. The speed of the rotor in metres per second can be calculated using Eq. (4);

$$L_V = RPM \times 1/60 \times 2\pi \times 0.05 \quad (4)$$

where L_V is the linear velocity measured in metres per second (m/s), and RPM is the number of revolutions per minute (rev/min).

The speed of the rotor was measured by a tachometer. This test was repeated 10 times to achieve an accurate measurement of the rotor speed. As the rotation of the rotor was 30 RPM, the linear velocity of the rotor while processing the flow of both powders was calculated using Eq. (4) and was found to be 0.157 m/s. This speed is constant throughout the whole printing process. The rotor in the feeder container rotates in both a clockwise and an anti-clockwise direction for each layer of printing. The period for which rotation occurs is approximately 16.5 s. Since the speed of the rotor was kept the same, both types of powders were thoroughly processed without any issues. It is important to identify the time period and speed of the rotor, particularly when attempting to check for harsh materials and when scaling up the size of a printer to produce large members for construction applications.

Table 6
Properties of gypsum powder (ZP 151) and cementitious powder (CP).

Powders properties	ZP 151	CP
Surface area (m^2/g)	0.999	1.021
Bulk density (g/cm^3)	0.912	0.79

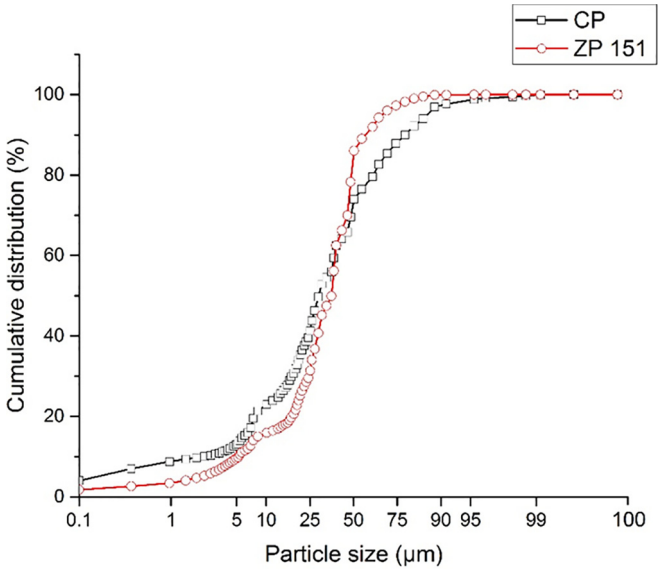

Fig. 5. Cumulative distribution of cement powder (CP) and gypsum powder (ZP 151).

UNCORRECTED PROOF

Please cite this article as: P. Shakor, S. Nejadi, G. Paul, et al., Dimensional accuracy, flowability, wettability, and porosity in inkjet 3DP for gypsum and cement mor..., Automation in Construction, https://doi.org/10.1016/j.autcon.2019.102964

ARTICLE IN PRESS

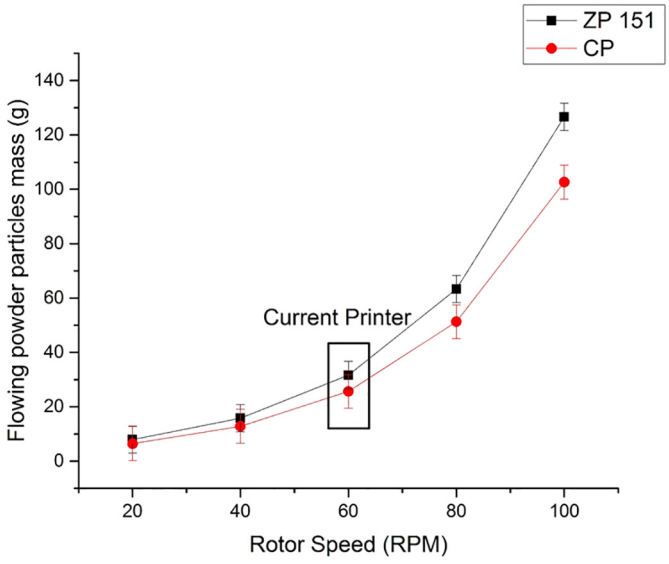

Fig. 6. The relationship between rotor speed (RPM) and the flowing powder particles mass (g).

Fig. 6 shows the predicted speed versus the particle flow for both powders. The figure shows that the flow rate increases proportionally with increases of the rotor speed. In particular, ZP 151 was observed to flow more easily and with greater consistency than the CP powder (see Video 1).

It was observed that the number of particles that pass through the holes of the feeder container (Fig. 4) when using ZP 151 was greater than for CP. This was reconfirmed after the process of spreading one layer for printing was repeated ten times. The results are shown in Table 7, in which particles pass through the holes of the feeder container. The short video at 1000 frames/s Optronis (CamRecorder 450 × 2) has been attached to show the flowability of the particles through the holes for both powders (see Videos 1 and 2).

3.3. Dimensional accuracy

The dimensional accuracy of a fabricated specimen defines the grade of approval between the manufactured part dimension and its designed specification.

The dimensional deviation ratio (DDR) can be used to compute the dimensional precision of printed structures, as in Eq. (5);

$$\mathrm{DDR} = \frac{L_P - L_{CAD}}{L_{CAD}} \times 100\% \quad (5)$$

where L_p is a real (printed) length value of the specimen, and L_{CAD} is the CAD model length value which is 20 mm for all three sides of the cube.

Table 8 presents the identified DDR value for all three axis orientations (X, Y, Z): the X-axis is the direction of the printhead that is parallel to the bed when it crosses the jet binder; the Y-axis is the direction of the bed that is perpendicular to the direction of the printhead; and the *Z*-axis is the direction of the next layer that is added on top of the previous layer. Each value is shown as an average (±) the standard deviation. As mentioned earlier (Section 3.1.2), the state of absorbing the binder liquid by the powder potentially affects the dimensions of the printed part. The dimensional accuracy of the fabricated part is affected by

Table 7
Weight of one spread layer on the feed chamber.

Spread layer	ZP 151 (g)	CP (g)
One spreading layer	15.83 ± 2.51	12.83 ± 3.12

Table 8
Difference between ZP 151 and CP in DDR for 3DP cubic specimen's saturation level (S170%C340%).

Cubic specimen	Dimensional deviation ratio (DDR) %		
	X-axis	Y-axis	Z-axis
ZP 151	3.75 ± 0.55	1.10 ± 0.60	2.25 ± 0.95
CP	−1.15 ± 0.11[a]	−3.9 ± 0.12[a]	0.7 ± 0.06

[a] The value with meaning specimen smaller than the original (CAD) drawing.

many factors such as wettability of the powder, surface morphology of the powder, binder reactivity with the powder, powder components, printing delay, build orientation, resolution of the printhead, post-processing procedures, binder droplet volume, layer thickness and particle size of the powder. In Table 8 there is a significant change in the Y-axis due to the printhead of the printer while distributing in the fast axis, overlapping the binder in the Y-axis. Another suspected reason for the Y-axis change is related to the penetration of the binder in the powder bed.

The major advantage of the inkjet 3DP technique is the ability to fabricate structural components with complicated geometries without requiring costly formwork. The most vital aspect that distinguishes the inkjet 3DP from a conventional casting method is the precision of printing. Fig. 7 shows the results of the dimensional accuracy of the green cubic specimen (green part) for the CP materials. Here, "green part" refers to a specimen that has been removed from the build chamber (build bin) prior to any post-processing.

The dimensional error for the mortar printed specimen (CP) can be found using Eq. (6):

$$D_e = D_p - D_{CAD} \quad (6)$$

where D_e is the dimensional error, D_p is the real printed dimension, and D_{CAD} is the original dimension from CAD. Fig. 7 also shows that, in general for all planes, the dimensional accuracy increases as the *w/c* is reduced. However, in the X-Y plane, a significant amount of undesirable deviation in the precision can be observed. These are lower than the nominal (CAD) dimensions due to the inaccuracy of the printhead nozzle and closeness of the nozzle. This inaccuracy could lead to overlapping and collisions of the binder when it drops on the powder. As mentioned earlier, the thermal DOD printhead works based on the thermal technology and an incorrect droplet dispersion would lead to a fault in the printed part. Further, the printhead nozzle sizes and errors in the positioning of the nozzle on the printhead have a significant influence on the dimensional accuracy of the printed parts. Another reason is the chemical and physical characterization of the powder-to-binder and the drop penetration ability of the powder. In addition, the printhead located on the fast axis rail has a high rate of movement. This fast rail at high movements can be reducing the accuracy of the dimensional part.

It is safe to assume that the dimensional accuracy of the 3DP parts is related to the orthotropic phenomenon, which has different mechanical strength results in each direction. The orthotropic properties of the printed objects are mainly related to the penetration of the liquid in the vertical Y-Z plane, which can be called the Z-direction of the specimen [52]. The X-Y plane has the highest variable error magnitude due to the liquid spreadability on the surface of the X-Y plane.

Despite the DDR shown in Table 8 for the ZP 151 specimen, ZP 151 has better shape stability and a more regular cubic appearance than CP specimens. Fig. 2 clearly shows the corners for each of the CP and ZP 151 specimens have different shapes. It is apparent that specimens made from ZP 151 have a more accurate appearance and uniform shape than the CP specimens. The filleting at the corners of CP specimens meant that it did not imitate the real shape of the cubic specimens. This phenomenon occurred in the CP specimens because of the shape of the powder particles in the CP specimens. Another reason is the powder

UNCORRECTED PROOF

Please cite this article as: P. Shakor, S. Nejadi, G. Paul, et al., Dimensional accuracy, flowability, wettability, and porosity in inkjet 3DP for gypsum and cement mor..., Automation in Construction, https://doi.org/10.1016/j.autcon.2019.102964

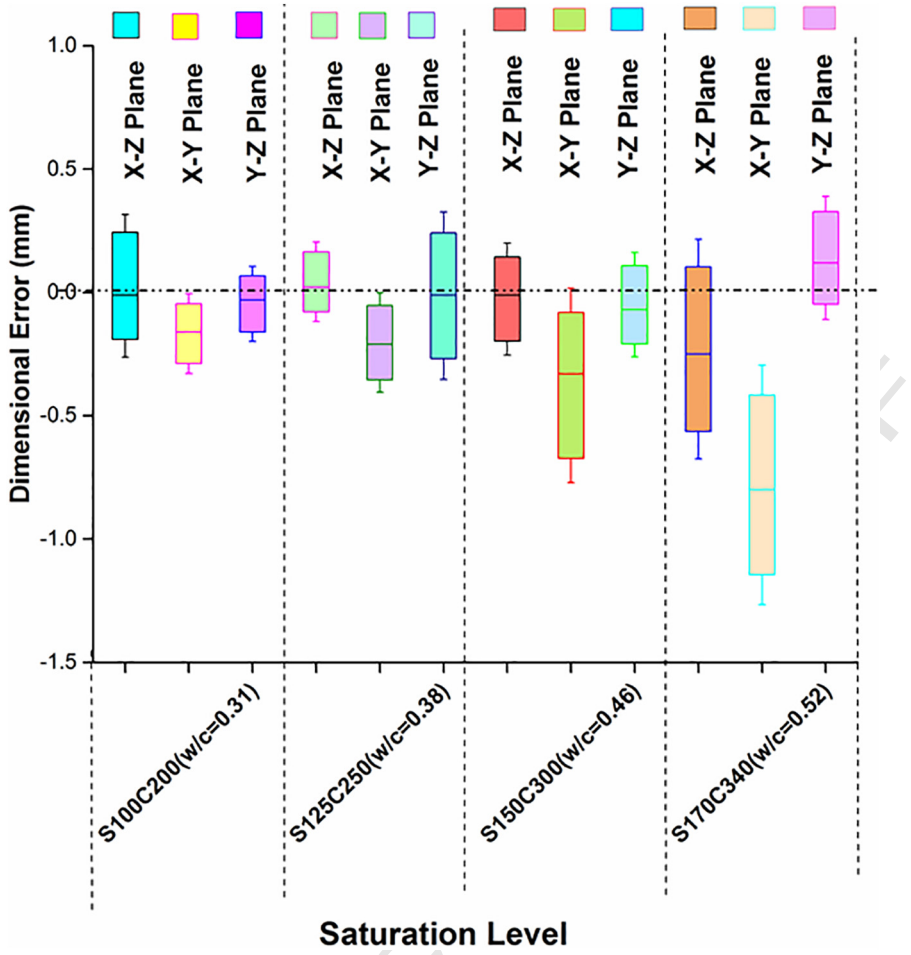

Fig. 7. The relationship between dimensional accuracy and saturation level (*w/c*) for printed green cube CP specimens (CAD 20 × 20 × 20 mm), printed by ProJet CJP (304 nozzles). (Note: the box is the mean ± standard deviation, and the whisker represents the ±minimum and maximum). (For interpretation of the references to colour in this figure legend, the reader is referred to the web version of this article.)

spreadability on the build chamber and binder reactions in the CP specimens that contain a greater number of voids and hygroscopic property. The reasons, which are explained in other subsections, are the flowability of powder, surface roughness and the apparent porosity of the specimens.

3.4. Flowability of the powder

The images of specimens from the laser microscope (*LEXT* OLS5000), show that the 3DP ZP 151 and CP specimens included micropores in the microstructure because of the large spacing between the particles, which ranged from 10 to 75 μm. Therefore, the flow for each of the powder particles fluctuates. Table 9 shows the surface roughness and topography of particles for each of the powders. The surface roughness on CP is much higher than ZP 151 due to numerous valleys on the powder bed. The roughness is related to the flow of the powder and rate that particles flow from the printer. Will et al. [53] stated that in the 3DP elements, the inter-agglomeration pores are generally formed in a size range of 1–100 μm, which is consistent with the observations of the present paper.

Table 9
Difference between ZP 151 and CP for the surface roughness for each of the powders.

Bedded powders on build chamber	Surface roughness (Ra) μm
ZP 151	12.72 ± 1.66
CP	19.83 ± 2.43

Methods used to calculate the flowability of the powders include Angle of repose, Carr's compressibility index, Hausner ratio flow through an orifice, the Shear cell method, and Cohesion index [54].

In this paper, the angle of repose for CP and ZP 151 has been found using Eq. (7);

$$\Theta = \arctan\frac{h}{D/2} \tag{7}$$

where Θ the angle of repose, h is the height of the pile, and D is the diameter of the base of the pile. Fig. 8 shows the angle of repose tests for both powders. The results for comparing the angles of repose of the commercial powder (ZP 151) and the modified powder (CP) are listed in Table 10. It has been found, that the regular process of fluidization in the powder reduced the agglomeration and the number of flowability issues in the CP powder. The fluidized bed process was verified with an initial trial and was consequently used as the standard powder preparation method for the study.

Yildirim [55] stated that an increment in the surface hydrophobicity of talc powder would lead to a decrease in the values of total surface free energy (γ_S) and the other components (γ_S^{LW} (apolar component) and γ_S^{AB}(polar component)), attributing this to the exposure of more basal plane surfaces upon pulverization. Further investigation is required to calculate the values of surface free energy for both CP and ZP 151.

There are several factors that decrease the flow of the powders: superficial adhesiveness, the shape of the particles (spherical particles flow quickly while irregular shape particles flow slowly), the surface

UNCORRECTED

Please cite this article as: P. Shakor, S. Nejadi, G. Paul, et al., Dimensional accuracy, flowability, wettability, and porosity in inkjet 3DP for gypsum and cement mor..., Automation in Construction, https://doi.org/10.1016/j.autcon.2019.102964

ARTICLE IN PRESS

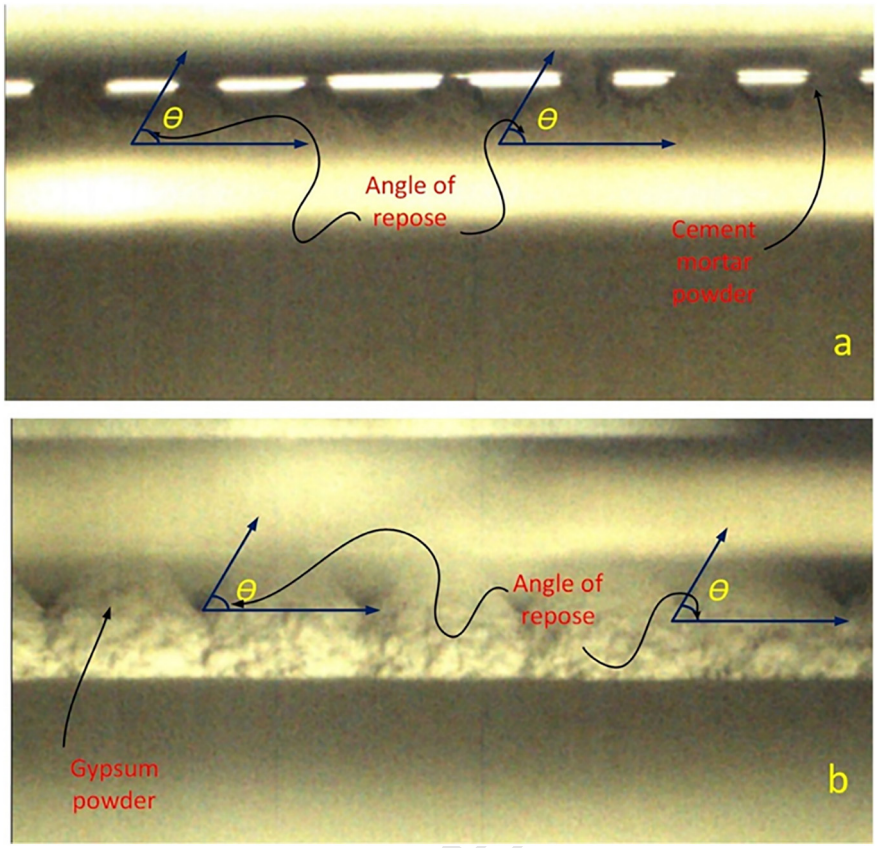

Fig. 8. Angle of repose for (a) CP powders after flowing from the feeder container of the printer, (b) ZP 151 powders after flowing from the feeder container of the printer.

of the particles (wrinkled surfaces have low flowability while smooth surfaces have a high flowability), the presence of the electrostatic charge on the surface, and the hygroscopicity of the powders. The electrostatic charges are generated inside the powder since when the particles flow they exchange charge when colliding with each other [56]. The charged particles in the powder experience electrostatic forces while in fluidized powder, most of the particles are likely to charge as a negative sign [56].

There are other approaches to calculate the flowability and cohesiveness of a powder, such as the Hausner ratio and Carr's index (see Table 11). Each of these approaches requires the tapped density and tapped volume of the powders. The bulk density is measured by dividing the mass by the untapped volume. The tapped density requires the mass to be divided by the tapped volume. The Hausner ratio can be calculated using Eq. (8);

$$H = \frac{V_t}{V_b} \tag{8}$$

where H is a Hausner ratio, V_t is tapped density, and V_b is a bulk density. A Hausner ratio of $H < 1.25$ indicates a powder that is free-flowing, whereas a ratio of $H > 1.25$ indicates poor flowability. For both powders, the Hausner ratio is >1.25. However, the modified CP powder has a much higher ratio than ZP 151.

Table 10
Difference between ZP 151 and CP for the angle of repose for each of the powders.

Powders	Angle of repose (Θ)°
ZP 151	53.90 ± 0.2
CP	70. 57 ± 0.4

Another approach is Carr's index, which is used to measure the flow properties of the powders. The Carr's index, I can be calculated using Eq. (9);

$$I = \frac{V_t - V_b}{V_t} \times 100 \tag{9}$$

where V_t is the tapped density, and V_b is the bulk density. A smaller Carr's Index means there are better flow properties. For instance, $5 < I \leq 12$ indicates "excellent", $12 < I \leq 16$ is "good", $16 < I \leq 23$ is "fair" and $23 < I$ is "poor" flow. Using this approach with both powders resulted in Carr's indices >23, thereby indicating poor flow. Nevertheless, the CP powder has a much higher cohesiveness and much poorer flow than the ZP 151 powder, recording 55.61% and 40.77%, respectively. It appears that both powders have low flow from the feeder container to the feeder chamber. However, the result shows that the flow for ZP 151 was better than for CP.

3.5. Wettability

Wettability or wetting is the ability of a fluid to maintain contact with a powder surface, as a result of the intermolecular interactions when the two are brought together. For example, fungi penetration

Table 11
Densities, Carr's index and Hausner ratio for the ZP 151 and CP powders.

Powders properties	ZP 151	CP
Surface area (m^2/g)	0.999	1.021
Bulk density (g/cm^3)	0.912	0.79
Tapped density (g/cm^3)	1.54	1.78
Hausner ratio = tapped density/bulk density	1.68	2.25
Carr's index = ((tapped density − bulk density) / tapped density) × 100	40.77%	55.61%

UNCORRECTED

Please cite this article as: P. Shakor, S. Nejadi, G. Paul, et al., Dimensional accuracy, flowability, wettability, and porosity in inkjet 3DP for gypsum and cement mor..., Automation in Construction, https://doi.org/10.1016/j.autcon.2019.102964

ARTICLE IN PRESS

time increases with decreasing pore size in the wood [57], with the velocity of fungus depending on the relationship between depth penetration and time taken.

The study of the presence of macrovoids in unpacked powder by Hapgood et al. [58] found that, for packed powder, the penetration will be easily and evenly distributed in the liquid. In their investigation, different liquid solutions were used with respect to time of penetration. One of the liquids with similar properties to Zb 63 is a clear binder solution named 3.5% HPC (Hydroxypropyl Cellulose) and dye. The penetration time for this solution was 21.5 s in the Merck lactose powder (d50 = 64.8 μm).

Another study by Doerr [59] explained the surface tension of water on soil. This study found that if a water droplet does not penetrate the soil, it means the surface tension of the soil is less than the surface tension of water (72.75 dynes/cm). Furthermore, the investigation stated that the porosity of the soil helps the water easily pass through the soil particles (hydrophilic soil) [60]. Earlier studies found that the porosity in the powder bed, fluid type and macrovoids all contribute to the wettability of the powder. Fig. 9 explains the penetration of the binder (water) into the ZP 151 at different stages of penetration.

Table 12 shows the highest spreading available in the CP. Thus, the penetration can be deduced as being due to the spreadability of the binder to the adjacent particle, rather than the depth of penetration into the powder. For example, Hapgood et al. [58] explained how large macrovoids would lead to a halt in the penetration of the droplet and instead result in spreading to the adjacent particles.

Fig. 10 explains the process of creating a bond between the two layers for ZP 151 due to the hydrophobic properties of the gypsum (ZP 151): the drop stays longer on the ZP 151 than on CP. Fig. 9 displays the image 16 s after the falling of the drop and the new layer bonded well due to the drop. According to the ZprinterManual [61], the vertical build speed takes 2 to 4 layers per minute. Thus, the photo was taken after 16 s for the purpose of showing the droplet as it is between layers. For this reason, the stopwatch timer and goniometer device were used for the printed specimens. The experimental results demonstrated the time between two layers for each printed specimen was approximately 16.64 ± 1.2 s. Therefore, taking the photo at 16 s is ideal to show the drop between the layers. The purpose of showing the binder drop between two layers in the ZP 151 is to show that the ZP powder has more powder packed on the build chamber than CP. The high number of voids in the cementitious powder (CP) allows the water binder to penetrate more quickly than in the recommended powder (ZP 151).

Table 12
Penetration time, the diameter of the droplet on the powder and depth of the penetration of the droplet.

Powder type	Droplet binder	Penetration time (s)	Diameter of the droplet (mm)	Depth of the penetrating droplet (mm)
ZP 151	Zb 63	55.24 ± 5.40	2.40 ± 0.09	1.25 ± 0.03
CP		3.70 ± 1.40	2.64 ± 0.02	1.11 ± 0.21

Capillary action is another factor that needs to be considered as it occurs between the surface of the packed bed and liquid solutions. According to the Young–Laplace Eq., the capillary pressure can be calculated using Eq. (10);

$$p_c = \frac{2\gamma\cos\theta}{r_c} \tag{10}$$

where p_c is capillary pressure, γ is surface tension, θ is the wetting angle and r_c the radius of the interface. This Eq. (10) shows the surface tension of the liquid directly related to capillary pressure. Therefore, a decrease in the surface tension of liquid will result in a reduction in the capillary pressure. As mentioned earlier, the surface tension of the binder liquid (0.00045 N/cm) used for the printing is lower than tap water (0.000728 N/cm). However, the capillary pressure of the binder liquid droplet has a lower capillary action for both powder bed surfaces (CP and ZP 151), due to the surface tension of the liquid.

Fig. 10 shows that the dropped binder (water) remained longer on the ZP 151 resulted in the droplet binding layers more effectively.

The graphs in Fig. 11, show the results of the three trials of contact angle goniometry (KSV CAM200) on the ZP 151 and CP. These graphs exhibit the time of penetration for each binder on the two different powders.

In Fig. 11, the water droplet could stay until the new layers of powder are deposited. It is clear from the graph that ZP 151 is more tightly packed than CP. In the graph, the volume of the water drop at 16.224 s is approximately 0.27 μl and the height is 0.25 mm. The height of each layer is 0.1 mm. The period taken for drop penetration into each layer is approximately 16.3 s. Thus, the figure shows that the droplet of water from the previous layer was still protruding when the roller deposited a new layer on the previous layer of powder. The printhead was then moving and the dripping of the binder over the powder

PROOF

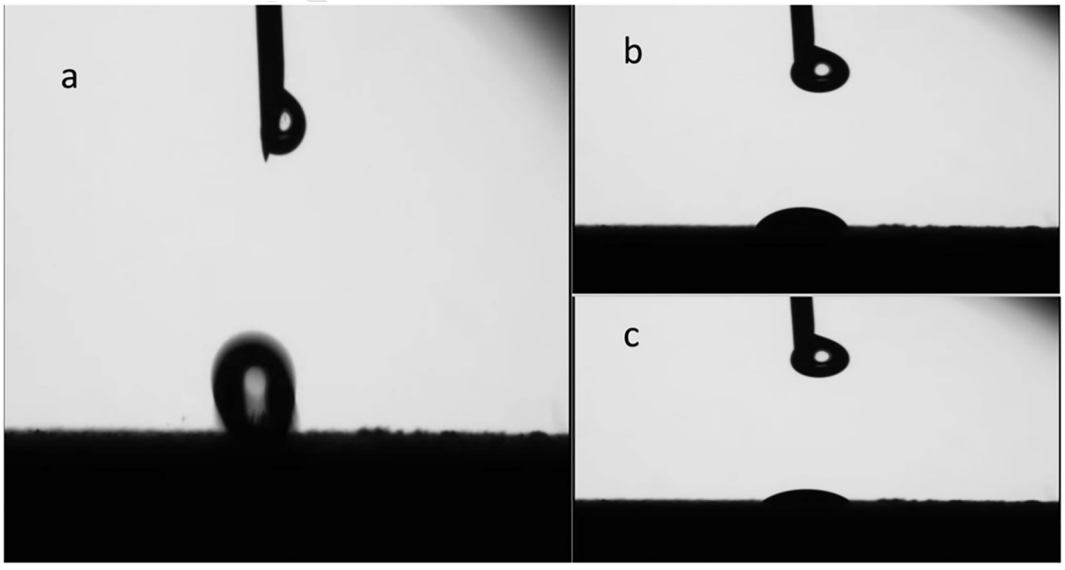

Fig. 9. Steps of Zb63 liquid penetrating into ZP 151, (a) impact time of droplet on the surface of the powder, (b) penetration processes of liquid on the powder after 16 s, (c) absorbing most of the liquid into the powder (after approximately 55 s).

Please cite this article as: P. Shakor, S. Nejadi, G. Paul, et al., Dimensional accuracy, flowability, wettability, and porosity in inkjet 3DP for gypsum and cement mor..., Automation in Construction, https://doi.org/10.1016/j.autcon.2019.102964

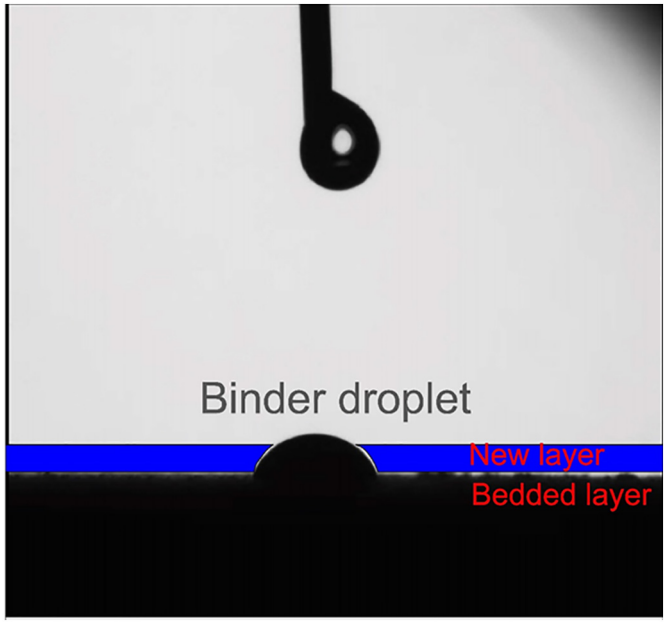

Fig. 10. Schematic explanation of a binder droplet between two layers and binding two layers together. The schematic shows what happens at the 16 s mark.

continued. Overall, this study found that ZP 151 has a tightly packed surface and particles are distributed evenly on the bed. On the other hand, the CP has more voids and porous space between the particles due to the agglomeration between cementitious powders and is less free-flowing from the container to the feeder chamber.

A measure of the contact angle is a proxy that can be used to measure wettability. For instance, Siebold et al. [62] stated that the contact angle has a higher value at all times during capillary rise than is anticipated, and depends firmly on increasing velocity. They also explored how the capillary rise was carried out at a single capillary and in column-packed powder to determine the contact angle.

There are a few investigations of the type of powders and penetration, such as using two types of powder for hydrophobicity and hydrophilicity. Salicylic acid and Lactose of 100 and 200 grade, respectively, were chosen for the hydrophobic and hydrophilic investigations [63]. The Salicylic acid particle sizes are smaller than the Lactose particles. Regarding particle size, the finer particles have been shown to exhibit hydrophobic properties [64]. They found that the penetration time increases with the addition of fine particles of salicylic acid to the powder mixture, which agrees with the present study. The evidence on penetration time is overwhelming and shows that hydrophobic properties will occur in fine powder particles.

The time between printing layers has a significant impact on the result of the printed part and correct wettability between printed layers. For example, Farzadi et al. [50] discovered that printing layers with different printing delays have an impact on the physical and mechanical properties of the printed structure.

Hydration and energy release have also a high impact on the material characterization results of the printed object. Research has found that the thickness of the calcium silicate hydrate (C-S-H) rims in cement in 28 day-old pastes increased from 5 mm to 25 mm at 20 °C and 80 °C, respectively [65]. C-S-H is the basic product in the hydration of Portland cement and is mainly responsible for the strength in cement-based materials. Energy dispersive spectroscopy microanalyses revealed that the chemical structures of the different C-S-H rims depend mostly on the temperature at which they were made. The lighter C-S-H made at 90 °C has a greater attraction in regard to sulphate than C-S-H developed at 20 °C (post- or pre-cured C-S-H produces). During the following storage at 20 °C, the release of sulphate from the lighter C-S-H gel designates that SO_4^{2-} is not chemically stuck in the C-S-H specimen but may be balanced and sorbed by Ca_2^{+} in the C-S-H during heat curing [66].

There is a strong relationship between the surface roughness (Ra) of the materials and the contact angle (wettability) of the surface of the powder. Two situations should be taken into account for the effect of roughness, namely, if the binder droplet leads to a groove in the surface or if air pockets are left between the droplet and the surface [67]. Fig. 12 shows the different surface roughness of the embedded powder on the build chamber of the 3DP. ZP 151 powder has a uniform distribution of particles on the surface. Conversely, CP powder has uneven distribution particles on the surface.

If the surface homogeneously becomes wet, the droplet is said to be in a Wenzel state. In a Wenzel state [68], wettability will be enhanced by adding surface roughness, which is affected by the chemistry of the surface. The Wenzel relationship can be written as Eq. (11);

$$\cos(\theta_m) = r \ \cos(\theta_Y) \tag{11}$$

where θ_m represents the contact angle, θ_Y is known as a Young contact angle, and r is called the roughness ratio.

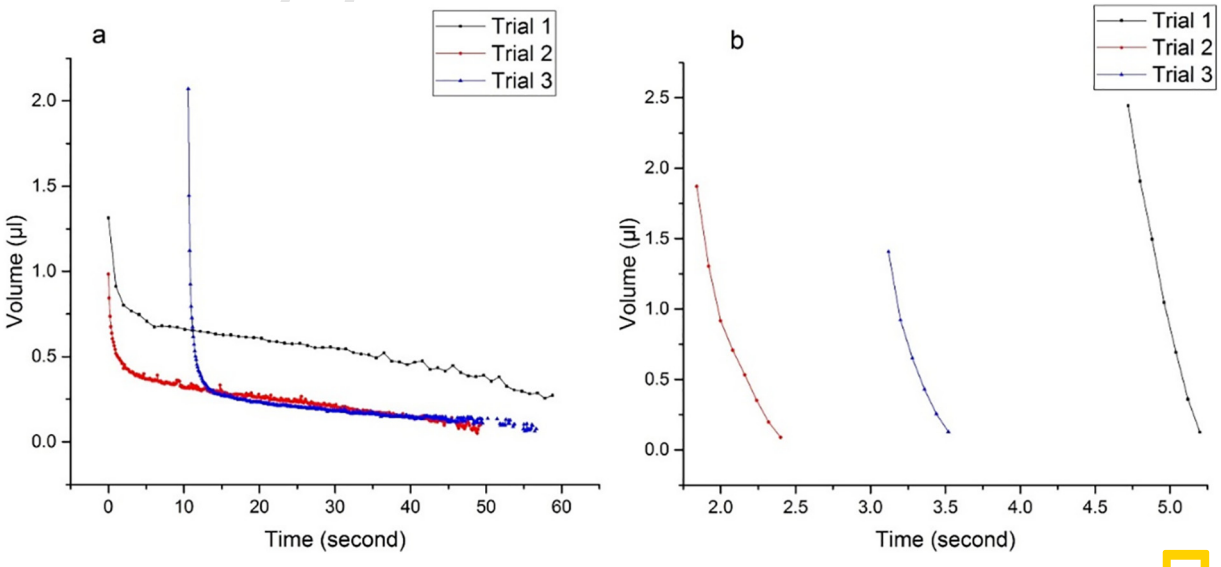

Fig. 11. (a) Penetration time per binder volume (µl) consumed in ZP 151, (b) penetration time per binder volume (µl) consumed in CP powder.

Please cite this article as: P. Shakor, S. Nejadi, G. Paul, et al., Dimensional accuracy, flowability, wettability, and porosity in inkjet 3DP for gypsum and cement mor..., Automation in Construction, https://doi.org/10.1016/j.autcon.2019.102964

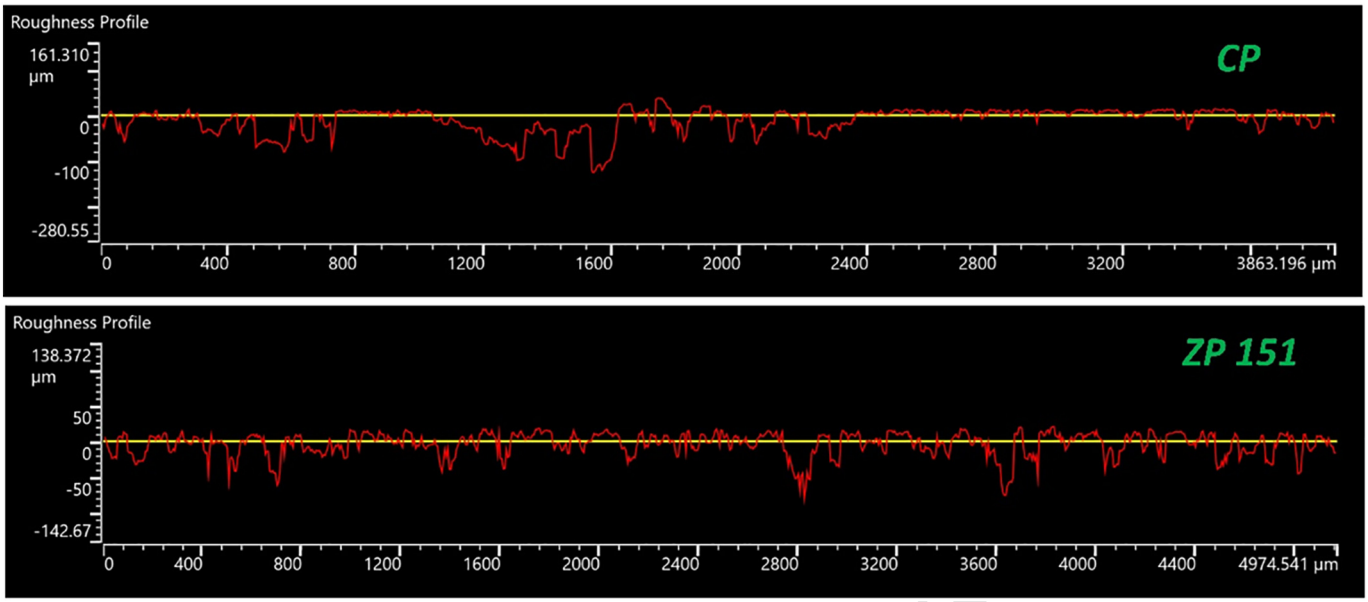

Fig. 12. Surface roughness profile for powder bed CP and ZP 151 materials.

However, when the surface becomes heterogeneously wet, the droplet is said to be in a Cassie-Baxter state [69]. The most stable contact angle is related to the Young contact angle. The contact angles have been considered from each of the Wenzel and Cassie-Baxter

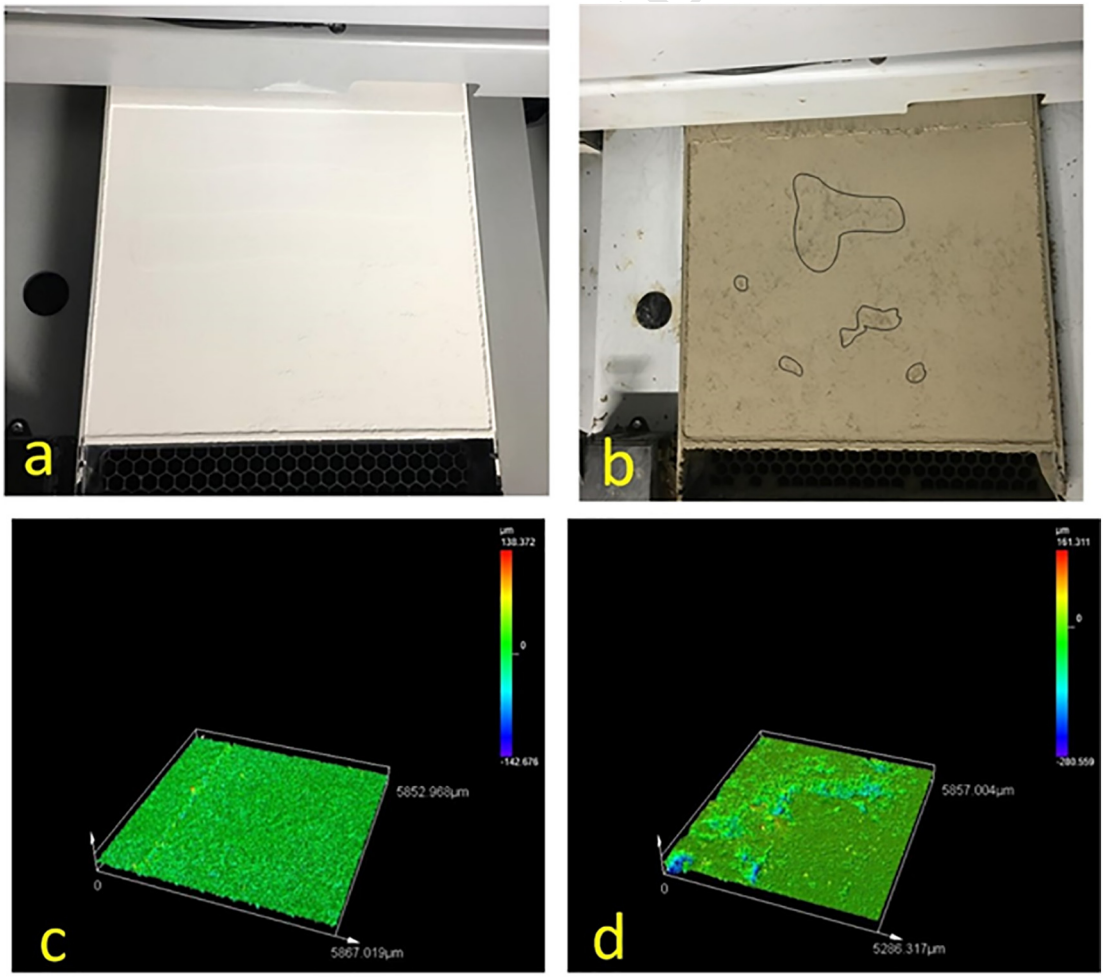

Fig. 13. The powder bed on the build chamber: (a) ZP 151 (gypsum) the powder on the build chamber, and (c) scan of the bed using the 3D scanner (Olympus OLS5000); and (b) CP (mortar) the powder on the build chamber, and (d) scanned powder bed using the 3D scanner.

Please cite this article as: P. Shakor, S. Nejadi, G. Paul, et al., Dimensional accuracy, flowability, wettability, and porosity in inkjet 3DP for gypsum and cement mor..., Automation in Construction, https://doi.org/10.1016/j.autcon.2019.102964

t13.1 **Table 13**
t13.2 Bulk density, in-process density and powder bed porosity.

t13.3 Powder properties	ZP 151	CP
t13.4 Bulk density (g/cm^3)	0.91	0.79
t13.5 True density (g/cm^3)	2.65	3.07
t13.6 In-process density (g/cm^3)	0.93	0.81
t13.7 Powder bed porosity (%)	64.9%	73.6%

Eqs. which was found to be a reasonable assumption for the most stable contact angles with real surfaces [70]. Thus, the most suitable Eq. for CP powder in inkjet 3DP, which could be measured as a heterogeneous wet surface, could be expressed as follows Eq. (12):

$$\cos\theta_w = f_1 \cos\theta_R - f_2 \quad (12)$$

where θ_R represents the solid-to-water declining contact angle, and θ_w is the apparent receding contact angle for the porous surface. It should be noted that f_1 and f_2 in Eq. (12) are designated by the advancing contact angle θ_A.

3.6. Powder bed porosity

The process of determining powder bed porosity requires finding the in-process bed density, (ρ_{bed}), as proposed by Zhou et al. [35], which measures the density after the powder is placed on the build chamber. The powder bedding should be of a high quality so that the inkjet 3DP technique can ensure high-quality printing results.

Fig. 13 shows the quality surface of the ZP 151 and CP powders. The visual inspections and 3D laser scanning show the porosity and voids on the surface of the powder. At the top of Fig. 13(a, b), the powder is bedded on the build chamber and the photo was taken for visual inspection to identify any differences between the powders. However, the bottom of Fig. 13(c, d), which illustrates the same final bedded layer after being scanned by the 3D laser scanner, shows that the CP powder has a lower quality surface roughness and the powder is distributed unevenly. The selected surface that has been scanned has an area approximately (5857 × 5286)μm and (5852 × 5867)μm for CP and ZP 151, respectively.

The surface roughness of both powder beds has been measured using an Olympus (LEXT OLS5000), (see Table 9). The results show that the ZP 151 powder bed surface roughness is approximately 12.72 ± 1.66 μm and the surface roughness for CP is approximately 19.83 ± 2.43 μm. Table 13 shows the result of powder bed porosity, namely, 73.6% in the CP and 64.9% in the ZP 151. Therefore, the final product of the CP printed specimens would have a higher porosity than ZP 151. Hence, the powder bed porosity has a great influence on the solid printed product, and the porosity of the powder bed is directly related to the printed specimens.

3.7. Porosity in the specimen

The previous subsection discussed powder bed porosity. This bed porosity directly affects the porosity in the specimens. Fig. 14 shows the result of the porosity of 3DP specimens for different saturation levels while using lithium carbonate and without lithium carbonate. The lower level of porosity was noted at the saturation levels of the specimen (S170-C340). Fig. 14 shows that adding lithium carbonate by a small amount has a positive impact on the porosity of the printed powder at saturation level of (S125%C250%). However, the porosity at the highest and lowest saturation levels for both mixes is almost the same. The minimum porosity in the specimen was 55.23 ± 0.25%.

Fig. 15 shows the fluctuation of porosity versus compressive strength while increasing the *w/c* ratio [16]. When porosity decreased, the compressive strength increased slightly, which was the expected result. In general, having a high degree of porosity weakens concrete strength. The results in Fig. 15 refer to a printed part without extra curing, such as heat post-processing. It shows that while the porosity reduces relative to increasing in saturation level (S150%C300%), the compressive strength increases again with the error bar value higher than the other specimens. The result recorded 2.86 ± 0.23 MPa, 2.82 ± 0.10 MPa for (S170%C340%) and (S150%C300%), respectively. This is expected since the ratio of water (saturation level) increasing in the specimens, which then enhances the compressive strength of the specimens. However, the porosity in the 3DP specimens usually decreases with increased amounts of water in the printed specimens, which

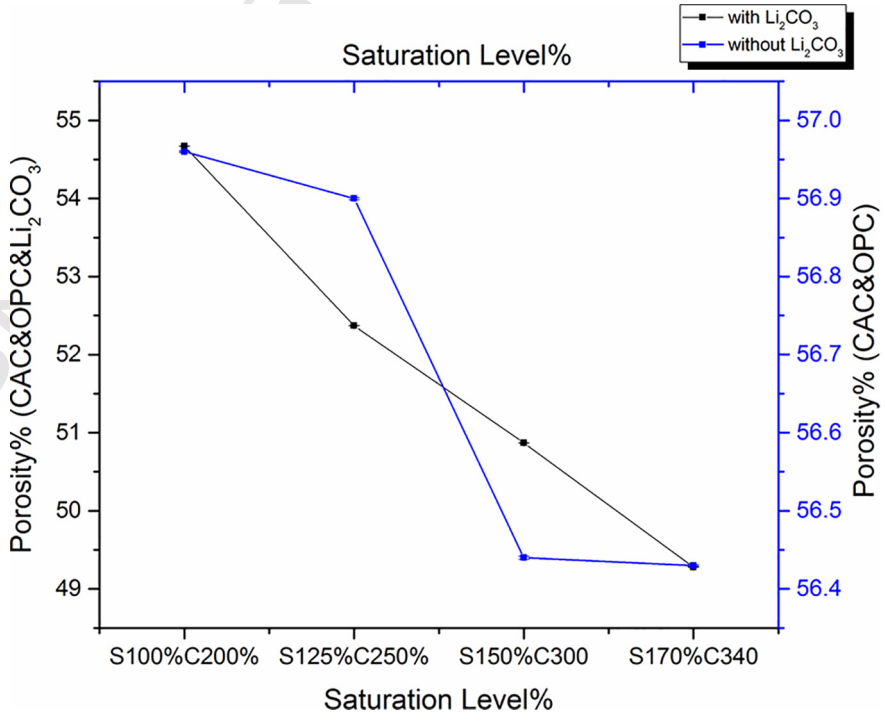

Fig. 14. Porosity versus saturation level for specimens CP with/without lithium carbonate

UNCORRECTED PROOF

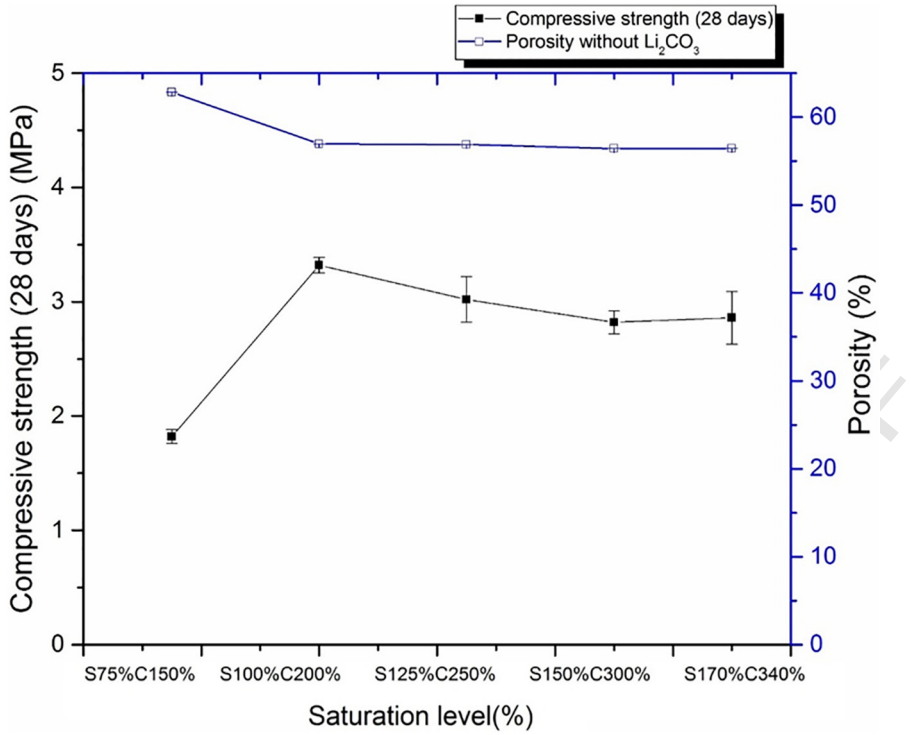

Fig. 15. Compressive strength versus saturation levels for CP specimens without lithium carbonate and without heat post-processing.

indicates that the part has been saturated fully and has enhanced the reaction among particles in a fully saturated state, as clarified in [16].

In general, the compressive strength improves with an increase to the *w*/*c* ratio, and reduces the apparent porosity from 62.85% to 55.23%, while saturation levels change from (S75%C150%) to (S170% C340%). Increasing the saturation levels and reducing porosity causes a better reaction and crystalize the cementitious particles, which in turn makes a stronger bond for the printed specimens. Test results

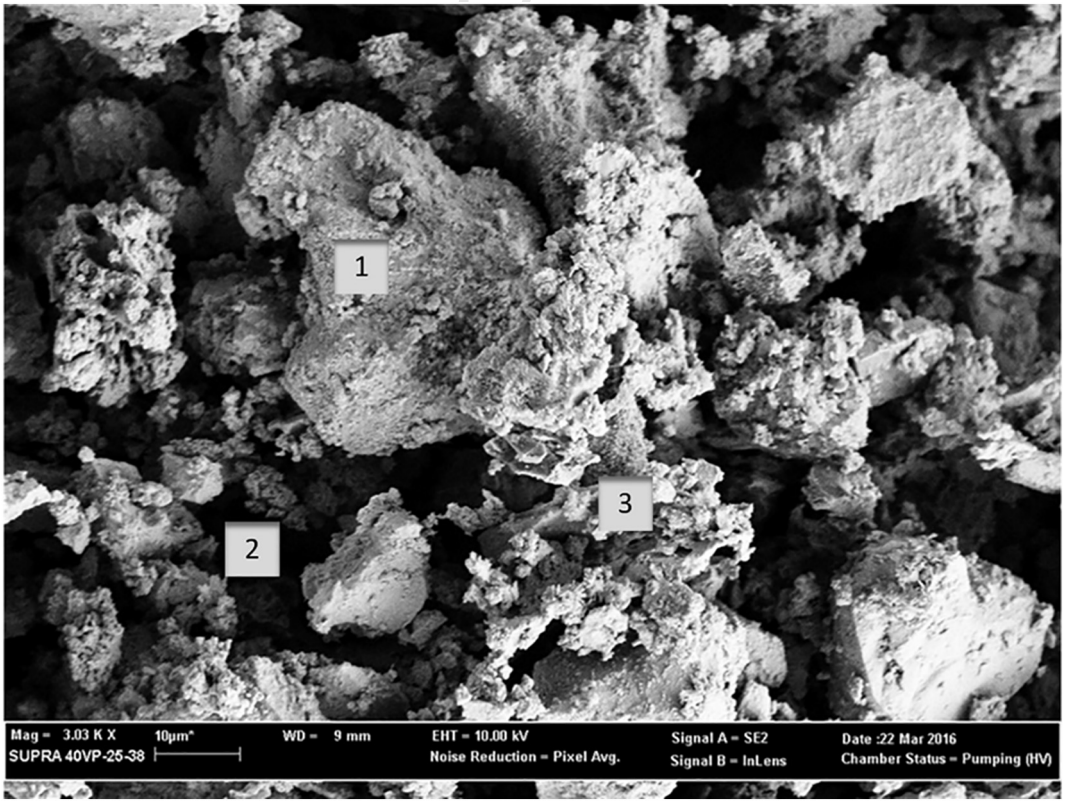

Fig. 16. Image of Scanning Electron Microscope (10 µm) for the 3DP (green part) CP specimen. (For interpretation of the references to colour in this figure legend, the reader is referred to the web version of this article.)

Please cite this article as: P. Shakor, S. Nejadi, G. Paul, et al., Dimensional accuracy, flowability, wettability, and porosity in inkjet 3DP for gypsum and cement mor..., Automation in Construction, https://doi.org/10.1016/j.autcon.2019.102964

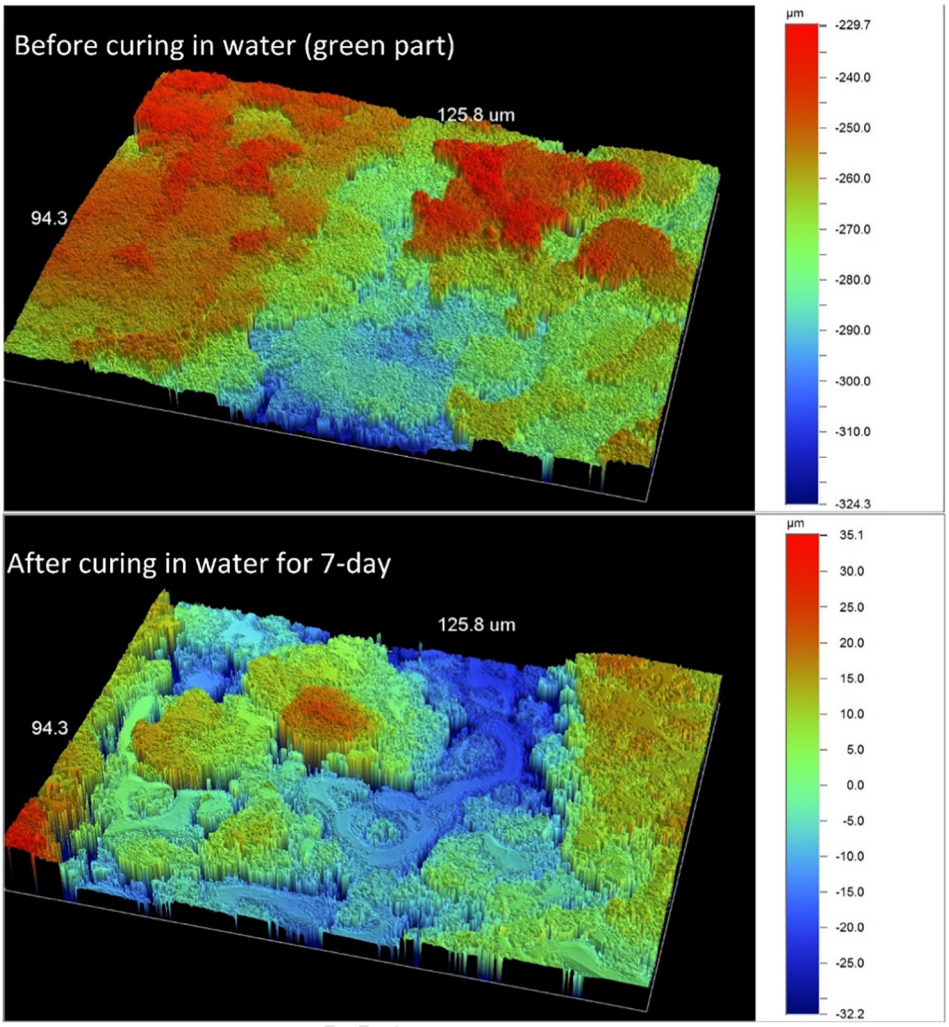

Fig. 17. 3D scanned image (50×) of the printed CP specimen before curing (green part) and after curing in water for 7 days. (For interpretation of the references to colour in this figure legend, the reader is referred to the web version of this article.)

have been recorded for the specimens that are cured in tap water without further post-processing (e.g. no heat curing). Lowke et al. [15] stated that the layer thickness, liquid jet pressure and post-treatment are major parameters affecting the resulting printed parts. This has been confirmed in the earlier works of Pierre et al. [71], which show the full penetration parts has a homogenous and better bond between layers.

Post-processing, such as heat curing, infiltration (e.g. waxing, dipping in resin) has been shown to affect the mechanical strength of the printed specimens. Post-processing is regularly applied in the field of biomaterials and food processing to increase the efficiency of the behaviour of the material [72].

Fig. 16 illustrates the test executed using a Scanning Electronic Microscope (SEM), which shows the voids among particles of the printed specimen and open pores between particles. The large crystal plate-likes growths occurred while unreacted particles can be seen on the surface of the specimens. It shows that there are deep voids and incohesive particles on the printed specimen (black colour number 2 in Fig. 16). Clearly, the process of hydration has not been accomplished between some of the cement powder particles and has left many voids between particles. The 3D scanning profile has assisted in identifying the porosity in the specimens.

Fig. 16 number 1 is a large crystal which represents the fine sand, and number 3 represents the crystal C-S-H formation of the cementitious materials.

As shown in Fig. 17, the saturation levels of specimens with various magnifications have been examined to determine the surface roughness and porosity of the specimens. The test was conducted using a 3D scanner, Veeco (Dektak), and an Olympus (*LEXT* OLS5000) with 50× magnifications. In Fig. 17 the porosity and the uneven surface on the printed specimens are visible. The specimens were tested and zoomed-in to the side layer (XZ-plane) for the green part, and then specimens were cured in water (refer to Fig. 16). After 7 days of being cured in water, specimens were scanned using the 3D scanner to visualise and measure the valleys (porous holes) on the surface. The topology and height distributions dramatically changed. These changes can be observed by means of the value of skewness (*Ssk*), which is a parameter linked with porosity and load bearing. Petzing et al. [73] explained that a *Ssk* value of zero means that the height distribution at the surface is symmetrical. This is proved by the centre line for both asymmetrical and symmetrical purposes. After curing, the specimens have an asymmetric end extending out toward the more positive sign, which means many

Table 14 t14.1
Skewness value for the CP specimens before and after 7 days of curing in tap water. t14.2

Specimen description	*Ssk* value		t14.3
	Before curing (green part)	After curing in water (7 days)	t14.4
S100%C200%	−0.025	+0.364	t14.5

Please cite this article as: P. Shakor, S. Nejadi, G. Paul, et al., Dimensional accuracy, flowability, wettability, and porosity in inkjet 3DP for gypsum and cement mor..., Automation in Construction, https://doi.org/10.1016/j.autcon.2019.102964

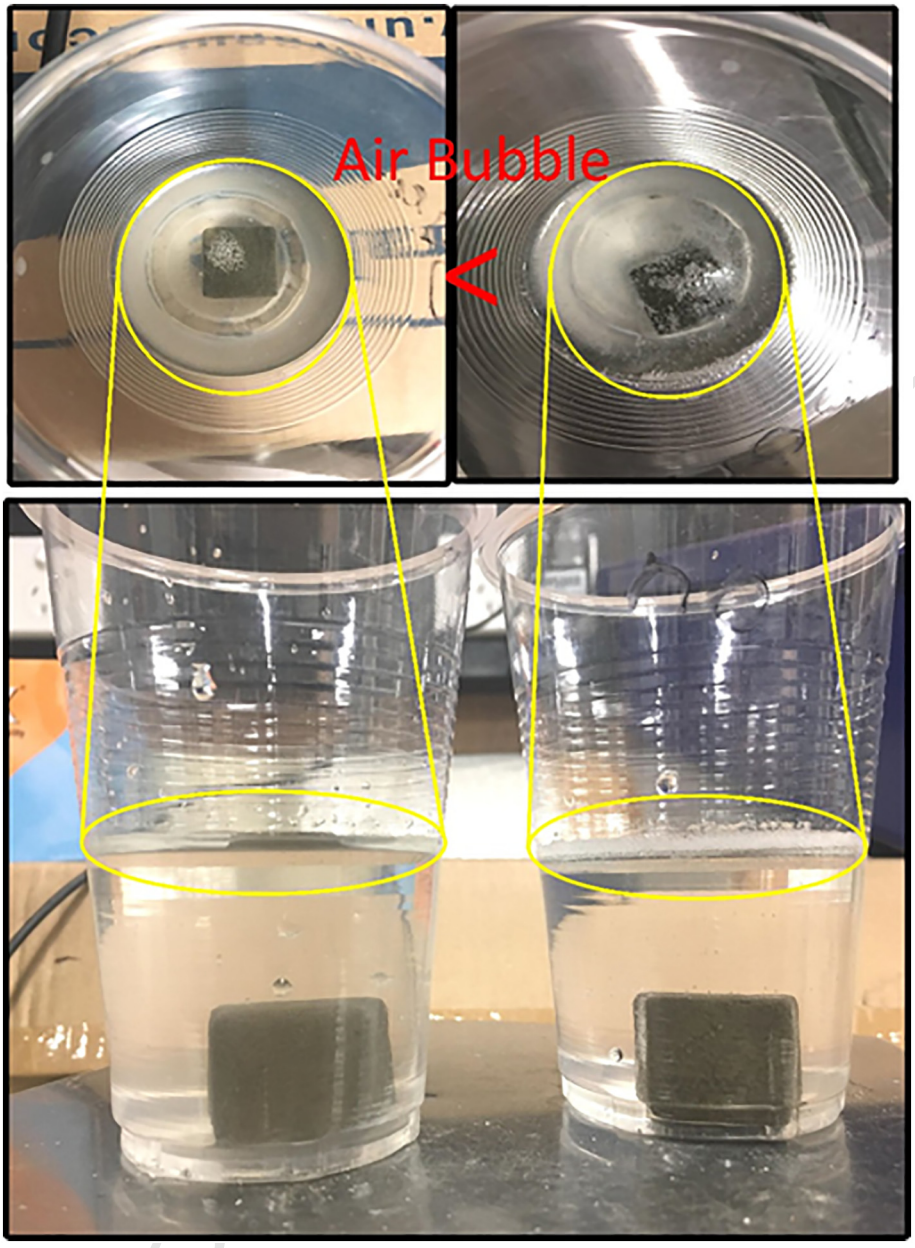

Fig. 18. The difference between curing in the oven for 3 h then inserting into water (left); not-curing in the oven then putting into water (right); there are more air bubbles (voids) on the right than the left.

high spikes emerged on the surface topography. As shown in Table 14, the direction of each skew is distinguished from the below the mean line, indicating a positive skew, or one above the mean line, indicating a negative skew. Table 14 shows the *Ssk* values for the printed specimen (S100%C200%) at the same spot before curing and after curing in tap water for 7 days. The value of skewness is dramatically changed from the negative skewness to positive skewness, due to the water's effect on the surface of the specimen. It can also be observed in Fig. 17 that

Table 15
Curing for 3 h in oven compared with not curing in the oven.

Specimen description	Medium of cure	Weight difference after water absorption (g)	Difference in weight for (non-cure minus cured specimen) (g)	Note
0 day	Non-cure	3.71	−0.22	Both specimens are kept for 3 h in water before weighing
	3 h cure in an oven	3.93		
1 day	Non-cure	7.94	+0.49	Both specimens are kept for 1 day in water before weighing
	3 h cure in an oven	7.45		
2 days	Non-cure	10.29	+0.63	Both specimens are kept for 2 days in water before weighing
	3 h cure in an oven	9.66		
3 days	Non-cure	12.65	+0.62	Both specimens are kept for 3 days in water before weighing
	3 h cure in an oven	12.03		

Please cite this article as: P. Shakor, S. Nejadi, G. Paul, et al., Dimensional accuracy, flowability, wettability, and porosity in inkjet 3DP for gypsum and cement mor..., Automation in Construction, https://doi.org/10.1016/j.autcon.2019.102964

ARTICLE IN PRESS

many of the particles are released from the surface because they evidently did not have perfect reactions and hydrations in the printing process, specifically in low water/cement ratio (i.e. saturation level).

Fig. 17 demonstrates that the specimens detach and released many particles. Thus, valleys (porous holes) have emerged on the surface of the specimens that are cured in water. The porosity in CP is higher than in ZP 151 because the binder droplet penetration time is quicker, see Fig. 11.

Post-processing or curing has a major impact on the results of mechanical strength and the hydration process of the printed powder. Fig. 18 shows the air bubbles in the uncured specimen in the oven are higher than in the specimen that was cured in an oven for 3 h at (60 °C). This indicates that the curing process with heat resulted in improved printed specimens by reducing the voids and porosity between printed layers.

In Fig. 18 the specimen on the left has been cured in the oven for 3 h at (60 °C) and the specimen on the right was not cured in an oven. The results show that the water absorption in the non-cured specimen in the oven was higher than the specimen cured in the oven. Table 15 shows the weight results from the first until the third day of curing in water for both specimens. Therefore, this shows that the rate of porosity is greater in the non-cured specimen than it was for the specimen cured in the oven. Earlier studies found that curing concrete in a medium substituting 2% of TiO_2 nanoparticles significantly increased the flexural strength and reduced the percentage of water that is absorbed by the specimens [74]. This means reducing the water absorption by the specimens has a positive effect on the mechanical strength of the specimens. Such studies need further investigation to determine the precise nature of the voids, such as the proximity, distribution and size of the close pores inside the specimens. To find details of the precise voids in the printed specimens it is suggested that techniques such as X-ray computed tomography, μCT imaging or neutron beam could be used.

4. Conclusion

A study was conducted to compare the commercial powder (ZP 151) to modified cementitious powder (CP) for inkjet 3DP in terms of flowability, spreading powder, binding between layers, wettability, porosity and surface roughness. The results show that CP is printable and this combination of inkjet 3DP technique and CP are suitable for construction applications. The principal conclusions of this paper are as follows:

- The dimensional accuracy of the green-part of specimens in all three axes have been measured and shown to closely match the CAD model.
- The flowability of ZP 151 and CP powders have been compared by examining the repose angle, Hausner ratio and Carr's index. The results show that the CP powder has higher values of repose angle, Hausner ratio and Carr's index than those of ZP 151.
- Increasing the *w/c* ratio (or saturation levels as referred to in 3DP) resulted in an improvement in the compressive strength of the printed specimen. The maximum saturation level (S170%C340%) also corresponded to the highest compressive strength. In a traditional concrete mix, an increase in the *w/c* ratio is expected to reduce the strength of the concrete and increase the porosity and voids in the concrete. However, this paper has shown the contrary is true in 3DP, with a high *w/c* ratio achieving both high compressive strength and the lowest apparent porosity.
- The powder bed porosity in CP and ZP 151 are 73.6% and 64.9%, respectively. The apparent porosity in the specimens is related to the powder bed porosity. Addition of a small quantity of lithium carbonate showed a positive impact on the porosity results at a saturation level of (S170%C340%) and contributed to a slight improvement in the compressive strength of the specimens.
- The wetting and contact angle of binder (water) on CP powder recorded a higher spreading than on the ZP 151 powder.
- Assessment of the surface properties (e.g. roughness, skewness value, and porosity) of printed specimens under different curing conditions, using 3D scanning and SEM images, revealed that CP specimens had more roughness than ZP 151.

Further research is still required to more thoroughly investigate several aspects: (a) the movement of the binder droplets as they are dripped from the printhead, (b) the effect of delay time between bedded layers on mechanical properties, and (c) the impact of orientational angle of the printed specimens in the build chamber of the printer on mechanical properties. Additionally, it would be advantageous to consider different formulations of powder bed materials in inkjet 3DP.

Supplementary data to this article can be found online at https://doi.org/10.1016/j.autcon.2019.102964.

Acknowledgement

The authors would like to thank the staff at the civil engineering laboratory and ProtoSpace at the University of Technology Sydney for their support. The authors would also like to express their gratitude to Kerneos Australia Pty Limited providing the CAC. Q6

References

[1] AS1774.5:2014, Refractories and refractory materials - physical test methods, Method 5: Determination of Bulk Density, Apparent Porosity and True Porosity (ISO 5017:2013, MOD) Australia, ISBN: 978-1-74342-917-4, 2014.
[2] R. Bjorhovde, A. Colson, J. Brozzetti, Classification system for beam-to-column connections, Journal of Structural Engineering 116 (11) (1990) 3059–3076, https://doi.org/10.1061/(ASCE)0733-9445(1990)116:11(3059).
[3] J.G. MacGregor, J.K. Wight, S. Teng, P. Irawan, Reinforced Concrete: Mechanics and Design, Prentice Hall, Upper Saddle River, NJ, 1997. https://trove.nla.gov.au/work/9614219.
[4] T.D. Ngo, A. Kashani, G. Imbalzano, K.T. Nguyen, D. Hui, Additive manufacturing (3D printing): a review of materials, methods, applications and challenges, Composites Part B: Engineering (2018) https://doi.org/10.1016/j.compositesb.2018.02.012.
[5] M. Hambach, D. Volkmer, Properties of 3D-printed fiber-reinforced Portland cement paste, Cement and Concrete Composites 79 (2017) 62–70, https://doi.org/10.1016/j.cemconcomp.2017.02.001.
[6] B. Panda, S.C. Paul, M.J. Tan, Anisotropic mechanical performance of 3D printed fiber reinforced sustainable construction material, Materials Letters 209 (2017) 146–149, https://doi.org/10.1016/j.matlet.2017.07.123.
[7] N. Hack, W.V. Lauer, Mesh-mould: robotically fabricated spatial meshes as reinforced concrete formwork, Architectural Design 84 (3) (2014) 44–53, https://doi.org/10.1002/ad.1753.
[8] C. Gosselin, R. Duballet, P. Roux, N. Gaudillière, J. Dirrenberger, P. Morel, Large-scale 3D printing of ultra-high performance concrete – a new processing route for architects and builders, Materials & Design 100 (2016) 102–109, https://doi.org/10.1016/j.matdes.2016.03.097.
[9] J.-Y. Lee, J. An, C.K. Chua, Fundamentals and applications of 3D printing for novel materials, Applied Materials Today 7 (2017) 120–133, https://doi.org/10.1016/j.apmt.2017.02.004.
[10] T. Wangler, E. Lloret, L. Reiter, N. Hack, F. Gramazio, M. Kohler, M. Bernhard, B. Dillenburger, J. Buchli, N. Roussel, Digital concrete: opportunities and challenges, RILEM Technical Letters 1 (2016) 67–75, https://doi.org/10.21809/rilemtechlett.2016.16.
[11] Y.W.D. Tay, B. Panda, S.C. Paul, N.A. Noor Mohamed, M.J. Tan, K.F. Leong, 3D printing trends in building and construction industry: a review, Virtual and Physical Prototyping 12 (3) (2017) 261–276, https://doi.org/10.1080/17452759.2017.1326724.
[12] S. Azhar, Building information modeling (BIM): trends, benefits, risks, and challenges for the AEC industry, Leadership and management in engineering 11 (3) (2011) 241–252, https://doi.org/10.1061/(ASCE)LM.1943-5630.0000127.
[13] D. Bryde, M. Broquetas, J.M. Volm, The project benefits of building information modelling (BIM), International journal of project management 31 (7) (2013) 971–980, https://doi.org/10.1016/j.ijproman.2012.12.001.
[14] P. Shakor, S. Nejadi, G. Paul, S. Malek, Review of emerging additive manufacturing technologies in 3D printing of cementitious materials in the construction industry, Frontiers in Built Environment 4 (85) (2019) https://doi.org/10.3389/fbuil.2018.00085.
[15] D. Lowke, E. Dini, A. Perrot, D. Weger, C. Gehlen, B. Dillenburger, Particle-bed 3D printing in concrete construction – possibilities and challenges, Cement and Concrete Research (2018) https://doi.org/10.1016/j.cemconres.2018.05.018.
[16] P. Shakor, J. Sanjayan, A. Nazari, S. Nejadi, Modified 3D printed powder to cement-based material and mechanical properties of cement specimen used in 3D printing, Construction and Building Materials 138 (2017) 398–409, https://doi.org/10.1016/j.conbuildmat.2017.02.037.

UNCORRECTED PROOF

Please cite this article as: P. Shakor, S. Nejadi, G. Paul, et al., Dimensional accuracy, flowability, wettability, and porosity in inkjet 3DP for gypsum and cement mor..., Automation in Construction, https://doi.org/10.1016/j.autcon.2019.102964

ARTICLE IN PRESS

[17] V.N. Nerella, M.A.B. Beigh, S. Fataei, V. Mechtcherine, Strain-based approach for measuring structural build-up of cement pastes in the context of digital construction, Cement and Concrete Research 115 (2019) 530–544, https://doi.org/10.1016/j.cemconres.2018.08.003.

[18] A.V. Rahul, M. Santhanam, H. Meena, Z. Ghani, 3D printable concrete: mixture design and test methods, Cement and Concrete Composites 97 (2019) 13–23, https://doi.org/10.1016/j.cemconcomp.2018.12.014.

[19] S.C. Paul, Y.W.D. Tay, B. Panda, M.J. Tan, Fresh and hardened properties of 3D printable cementitious materials for building and construction, Archives of Civil and Mechanical Engineering 18 (1) (2018) 311–319, https://doi.org/10.1016/j.acme.2017.02.008.

[20] Y.W.D. Tay, G.H.A. Ting, Y. Qian, B. Panda, L. He, M.J. Tan, Time gap effect on bond strength of 3D-printed concrete, Virtual and Physical Prototyping 14 (1) (2019) 104–113, https://doi.org/10.1080/17452759.2018.1500420.

[21] J. Xu, L. Ding, L. Cai, L. Zhang, H. Luo, W. Qin, Volume-forming 3D concrete printing using a variable-size square nozzle, Automation in Construction 104 (2019) 95–106, https://doi.org/10.1016/j.autcon.2019.03.008.

[22] B. Panda, S.C. Paul, N.A.N. Mohamed, Y.W.D. Tay, M.J. Tan, Measurement of tensile bond strength of 3D printed geopolymer mortar, Measurement 113 (2018) 108–116, https://doi.org/10.1016/j.measurement.2017.08.051.

[23] V.N. Nerella, S. Hempel, V. Mechtcherine, Effects of layer-interface properties on mechanical performance of concrete elements produced by extrusion-based 3D-printing, Construction and Building Materials 205 (2019) 586–601, https://doi.org/10.1016/j.conbuildmat.2019.01.235.

[24] E. Bassoli, A. Gatto, L. Iuliano, M. Grazia Violante, 3D printing technique applied to rapid casting, Rapid Prototyping Journal 13 (3) (2007) 148–155, https://doi.org/10.1108/13552540710750898.

[25] R. Rael, V. San Fratello, Developing Concrete Polymer Building Components for 3D Printing, www.rael-sanfratello.com/media/emerging_objects/papers/243.pdf 2011.

[26] P. Shakor, S. Nejadi, G. Paul, J. Sanjayan, A. Nazari, Mechanical properties of cement-based materials and effect of elevated temperature on three-dimensional (3-D) printed mortar specimens in inkjet 3-D printing, Materials Journal 116 (2) (2019) 55–67, https://doi.org/10.14359/51714452.

[27] A. Farzadi, M. Solati-Hashjin, M. Asadi-Eydivand, N.A. Abu Osman, Effect of layer thickness and printing orientation on mechanical properties and dimensional accuracy of 3D printed porous specimens for bone tissue engineering, PLoS One 9 (9) (2014), e108252. https://doi.org/10.1371/journal.pone.0108252.

[28] B. Derby, Inkjet printing of functional and structural materials: fluid property requirements, feature stability, and resolution, Annual Review of Materials Research 40 (1) (2010) 395–414, https://doi.org/10.1146/annurev-matsci-070909-104502.

[29] R. Verma, G. Kaushal, State of the art of powder bed fusion additive manufacturing: a review, in: L.J. Kumar, P.M. Pandey, D.I. Wimpenny (Eds.), 3D Printing and Additive Manufacturing Technologies, Springer Singapore, Singapore 2019, pp. 269–279, https://doi.org/10.1007/978-981-13-0305-0_23.

[30] J. Glasschroeder, E. Prager, M.F. Zaeh, Powder-bed-based 3D-printing of function integrated parts, Rapid Prototyping Journal 21 (2) (2015) 207–215, https://doi.org/10.1108/RPJ-12-2014-0172.

[31] Z. Liu, M. Zhang, B. Bhandari, Y. Wang, 3D printing: printing precision and application in food sector, Trends in Food Science & Technology 69 (2017) 83–94, https://doi.org/10.1016/j.tifs.2017.08.018.

[32] A. Butscher, M. Bohner, C. Roth, A. Ernstberger, R. Heuberger, N. Doebelin, P.R. von Rohr, R. Muller, Printability of calcium phosphate powders for three-dimensional printing of tissue engineering specimens, Acta Biomater 8 (1) (2012) 373–385, https://doi.org/10.1016/j.actbio.2011.08.027.

[33] J. Mei, M.R. Lovell, M.H. Mickle, Formulation and processing of novel conductive solution inks in continuous inkjet printing of 3-D electric circuits, IEEE transactions on electronics packaging manufacturing 28 (3) (2005) 265–273, https://doi.org/10.1109/TEPM.2005.852542.

[34] S. Ahmad, Reinforcement corrosion in concrete structures, its monitoring and service life prediction––a review, Cement and Concrete Composites 25 (4) (2003) 459–471, https://doi.org/10.1016/S0958-9465(02)00086-0.

[35] Z. Zhou, F. Buchanan, C. Mitchell, N. Dunne, Printability of calcium phosphate: calcium sulfate powders for the application of tissue engineered bone specimens using the 3D printing technique, Mater Sci Eng C Mater Biol Appl 38 (2014) 1–10, https://doi.org/10.1016/j.msec.2014.01.027.

[36] P. McEleney, G. Walker, J. Orr, N.J. Dunne, Investigations on drop penetration and wetting characteristics of powder-liquid systems in relation to the mixing of acrylic bone cement, International Journal of Nano and Biomaterials 3 (1) (2010) 20–35, https://doi.org/10.1504/IJNBM.2010.036105.

[37] B. Panda, S. Ruan, C. Unluer, M.J. Tan, Improving the 3D printability of high volume fly ash mixtures via the use of nano attapulgite clay, Composites Part B: Engineering 165 (2019) 75–83, https://doi.org/10.1016/j.compositesb.2018.11.109.

[38] M. Kalms, R. Narita, C. Thomy, F. Vollertsen, R.B. Bergmann, New approach to evaluate 3D laser printed parts in powder bed fusion-based additive manufacturing in-line within closed space, Additive Manufacturing 26 (2019) 161–165, https://doi.org/10.1016/j.addma.2019.01.011.

[39] X. Lin, T. Zhang, L. Huo, G. Li, N. Zhang, J. Liao, Preparation and application of 3D printing materials in construction, 27th Biennial Conference of the Concrete Institute of Australia, Melbourne, Australia, 2015. https://dura.com.my/press-release?download=18...concrete-institute-australia...2015.

[40] H. Miyanaji, S. Zhang, A. Lassell, A.A. Zandinejad, L. Yang, Optimal process parameters for 3D printing of porcelain structures, Procedia Manufacturing 5 (2016) 870–887, https://doi.org/10.1016/j.promfg.2016.08.074.

[41] 3DSystems, ZB63 Safety Data Sheet, https://au.3dsystems.com/materials/visijet-pxl/safety-data-sheets 2012.

[42] B. Utela, D. Storti, R. Anderson, M. Ganter, A review of process development steps for new material systems in three dimensional printing (3DP), Journal of Manufacturing Processes 10 (2) (2008) 96–104, https://doi.org/10.1016/j.jmapro.2009.03.002.

[43] A. Withell, O. Diegel, I. Grupp, S. Reay, D. de Beer, J. Potgieter, Porous ceramic filters through 3D printing, Innovative Developments in Virtual and Physical Prototyping: Proceedings of the 5th International Conference on Advanced Research in Virtual and Rapid Prototyping, Leiria, Portugal, 28 September-1 October, 2011, CRC Press, Leiria, Portugal 2011, p. 313. https://core.ac.uk/download/pdf/56362921.pdf.

[44] J.K. Prescott, R.A. Barnum, On powder flowability, Pharmaceutical technology 24 (10) (2000) 60–85(https://pdfs.semanticscholar.org/a258/5ce6e31a1a14f4e309b7cc95968c55766d6a.pdf).

[45] G. Gold, R.N. Duvall, B.T. Palermo, J.G. Slater, Powder flow studies II: effect of glidants on flow rate and angle of repose, Journal of Pharmaceutical Sciences 55 (11) (1966) 1291–1295, https://doi.org/10.1002/jps.2600551125.

[46] ASTM:B962-16, Standard Test Methods for Flow Rate of Metal Powders Using the Carney Funnel, 2016https://doi.org/10.1520/B0964-16.

[47] H. Zhang, H. Zhao, J. Chen, J. Li, J. Yu, J. Nie, Defect study of MgO-CaO material doped with CeO2, Advances in Materials Science and Engineering 2013 (2013) 5, https://doi.org/10.1155/2013/673786.

[48] AS1774.6-2001(R2013), Refractories and Refractory Materials - Physical Test Methods Determination of True Density, AS, Australia, 2013, ISBN 0-7337-3778-1.

[49] B.V. Antohe, D.B. Wallace, Acoustic phenomena in a demand mode piezoelectric ink jet printer, Journal of Imaging Science and Technology 46 (5) (2002) 409–414(ISSN: 1062-3701).

[50] A. Farzadi, V. Waran, M. Solati-Hashjin, Z.A.A. Rahman, M. Asadi, N.A.A. Osman, Effect of layer printing delay on mechanical properties and dimensional accuracy of 3D printed porous prototypes in bone tissue engineering, Ceramics International 41 (7) (2015) 8320–8330, https://doi.org/10.1016/j.ceramint.2015.03.004.

[51] Q. Huang, J. Zhang, A. Sabbaghi, T. Dasgupta, Optimal offline compensation of shape shrinkage for three-dimensional printing processes, IIE Transactions 47 (5) (2015) 431–441, https://doi.org/10.1080/0740817X.2014.955599.

[52] Y. Shanjani, Y. Hu, R.M. Pilliar, E. Toyserkani, Mechanical characteristics of solid-freeform-fabricated porous calcium polyphosphate structures with oriented stacked layers, Acta Biomaterialia 7 (4) (2011) 1788–1796, https://doi.org/10.1016/j.actbio.2010.12.017.

[53] J. Will, R. Detsch, A.R. Boccaccini, Structural and biological characterization of specimens, Characterization of Biomaterials, Elsevier 2013, pp. 299–310, https://doi.org/10.1016/B978-0-12-415800-9.00008-5.

[54] D. Geldart, E.C. Abdullah, A. Hassanpour, L.C. Nwoke, I. Wouters, Characterization of powder flowability using measurement of angle of repose, China Particuology 4 (3) (2006) 104–107, https://doi.org/10.1016/S1672-2515(07)60247-4.

[55] I. Yildirim, Surface Free Energy Characterization of Powders, Virginia Tech, 2001. http://hdl.handle.net/10919/27525.

[56] L. Zhang, X. Bi, J.R. Grace, Measurements of electrostatic charging of powder mixtures in a free-fall test device, Procedia Engineering 102 (2015) 295–304, https://doi.org/10.1016/j.proeng.2015.01.146.

[57] M.J. Fuhr, M. Schubert, C. Stührk, F.W. Schwarze, H.J. Herrmann, Penetration capacity of the wood-decay fungus Physisporinus vitreus, Complex Adaptive Systems Modeling 1 (1) (2013) 6, https://doi.org/10.1186/2194-3206-1-6.

[58] K.P. Hapgood, J.D. Litster, S.R. Biggs, T. Howes, Drop penetration into porous powder beds, Journal of Colloid and Interface Science 253 (2) (2002) 353–366, https://doi.org/10.1006/jcis.2002.8527.

[59] S.H. Doerr, On standardizing the 'water drop penetration time' and the 'molarity of an ethanol droplet' techniques to classify soil hydrophobicity: a case study using medium textured soils, Earth Surface Processes and Landforms 23 (7) (1998) 663–668, https://doi.org/10.1002/(SICI)1096-9837(199807)23:7<663::AID-ESP909>3.0.CO;2-6.

[60] M. Tschapek, Criteria for determining the hydrophilicity-hydrophobicity of soils, Zeitschrift für Pflanzenernährung und Bodenkunde 147 (2) (1984) 137–149, https://doi.org/10.1002/jpln.19841470202.

[61] ZprinterManual, User Manual ZP 150, ZP 250, php.scripts.psu.edu/users/j/r/jrh225/ZP150PowderGuide.pdf 2012.

[62] A. Siebold, M. Nardin, J. Schultz, A. Walliser, M. Oppliger, Effect of dynamic contact angle on capillary rise phenomena, Colloids and Surfaces A: Physicochemical and Engineering Aspects 161 (1) (2000) 81–87, https://doi.org/10.1016/S0927-7757(99)00327-1.

[63] T. Nguyen, W. Shen, K. Hapgood, Drop penetration time in heterogeneous powder beds, Chemical Engineering Science 64 (24) (2009) 5210–5221, https://doi.org/10.1016/j.ces.2009.08.038.

[64] K.P. Hapgood, J.D. Litster, R. Smith, Nucleation regime map for liquid bound granules, AIChE Journal 49 (2) (2003) 350–361, https://doi.org/10.1002/aic.690490207.

[65] H. Patel, C. Bland, A. Pool, The microstructure of steam-cured precast concrete, Advances in Cement Research 8 (29) (1996) 11–19, https://doi.org/10.1680/adcr.1996.8.29.11.

[66] C. Famy, K. Scrivener, A. Atkinson, A. Brough, Effects of an early or a late heat treatment on the microstructure and composition of inner CSH products of Portland cement mortars, Cement and Concrete Research 32 (2) (2002) 269–278, https://doi.org/10.1016/S0008-8846(01)00670-6.

[67] BiolinScientific, Influence of surface roughness on contact angle and wettability, https://cdn2.hubspot.net/hubfs/.../AT-TN-07-Surface-roughness-CA-wettability.pdf.

[68] R.N. Wenzel, Resistance of solid surfaces to wetting by water, Industrial & Engineering Chemistry 28 (8) (1936) 988–994, https://doi.org/10.1021/ie50320a024.

[69] A.B.D. Cassie, S. Baxter, Wettability of porous surfaces, Transactions of the Faraday Society 40 (0) (1944) 546–551, https://doi.org/10.1039/TF9444000546.

UNCORRECTED PROOF

Please cite this article as: P. Shakor, S. Nejadi, G. Paul, et al., Dimensional accuracy, flowability, wettability, and porosity in inkjet 3DP for gypsum and cement mor..., Automation in Construction, https://doi.org/10.1016/j.autcon.2019.102964

ARTICLE IN PRESS

[70] A. Marmur, Solid-surface characterization by wetting, Annual Review of Materials Research 39 (1) (2009) 473–489, https://doi.org/10.1146/annurev.matsci.38.060407.132425.
[71] A. Pierre, D. Weger, A. Perrot, D. Lowke, Penetration of cement pastes into sand packings during 3D printing: analytical and experimental study, Materials and Structures 51 (1) (2018) 22, https://doi.org/10.1617/s11527-018-1148-5.
[72] J. Sun, Z. Peng, L. Yan, J.Y. Fuh, G.S. Hong, 3D food printing—An innovative way of mass customization in food fabrication, International Journal of Bioprinting 1 (1) (2015) 27–38, https://doi.org/10.18063/IJB.2015.01.006.
[73] J.N. Petzing, J.M. Coupland, R.K. Leach, The Measurement of Rough Surface Topography Using Coherence Scanning Interferometry, https://dspace.lboro.ac.uk/dspace-jspui/handle/2134/13271 2010.
[74] A. Nazari, The effects of curing medium on flexural strength and water permeability of concrete incorporating TiO2 nanoparticles, Materials and Structures 44 (4) (2011) 773–786, https://doi.org/10.1617/s11527-010-9664-y.

UNCORRECTED PROOF

Please cite this article as: P. Shakor, S. Nejadi, G. Paul, et al., Dimensional accuracy, flowability, wettability, and porosity in inkjet 3DP for gypsum and cement mor..., Automation in Construction, https://doi.org/10.1016/j.autcon.2019.102964